REPUBLIC OF TURKEY
YILDIZ TECHNICAL UNIVERSITY
GRADUATE SCHOOL OF NATURAL AND APPLIED SCIENCES

THE ZERO CONTROL OF LINEAR INDUCTION MOTOR DRIVEN MAGNETIC LEVITATED SUSPENSION

AHMET FEVZİ BOZKURT

MSc. THESIS
DEPARTMENT OF MECHATRONICS ENGINEERING
PROGRAM OF MECHATRONICS ENGINEERING

ADVISER
ASSIST. PROF. DR. KADİR ERKAN

İSTANBUL, 2016

REPUBLIC OF TURKEY
YILDIZ TECHNICAL UNIVERSITY
GRADUATE SCHOOL OF NATURAL AND APPLIED SCIENCES

THE ZERO CONTROL OF LINEAR INDUCTION MOTOR
DRIVEN MAGNETIC LEVITATED SUSPENSION

A thesis submitted by Ahmet Fevzi BOZKURT in partial fulfillment of the requirements for the degree of **MASTER OF SCIENCE** is approved by the committee on 25.07.2016 in Department of Mechatronics Engineering.

Thesis Adviser
Assist. Prof. Dr. Kadir ERKAN
Yıldız Technical University

Approved By the Examining Committee
Prof. Dr. Ekrem YANMAZ
Gelişim University   _____

Assist. Prof. Dr. Kadir ERKAN
Yıldız Technical University   _____

Assist. Prof. Dr. Hüseyin ÜVET
Yıldız Technical University   _____

ACKNOWLEDGEMENTS

I personally want to thank my thesis advisor Assist. Prof. Dr. Kadir ERKAN, whom kindness and vulnerable effort lead this study to success. Without the patient he showed me, this thesis cannot be completed.

Also our team gave me courage to work harder and further to accomplish this study. We worked together to make dreams come true. Their help cannot be forsaken, I want to thank them all.

And other friends, thanks.

Finally, I must thank my family for their support on every level of my life. Years of study could be happen because of their belief in me.

July 2016,

Ahmet Fevzi BOZKURT

TABLE OF CONTENTS

CHAPTER 4

MANUFACTURING PROCESS

CHAPTER 5

EXPERIMENTAL RESULTS 54

LIST OF SYMBOLS

α	alpha axis angular displacement
β	beta axis angular displacement
τ	Time equivalent constant
γ	Stability index
λ	Magnetic flux
φ	Flux density
R	Resistance of coil
L	Inductance of coil
N	Turn of coil
S	Cross section of electromagnet
μ0	Magnetic flux permeability
m	Mass
g	Gravitational acceleration
Jα	alpha axis moment of inertia
Jβ	beta axis moment of inertia
fd	Disturbance force
fdz	z – axis disturbance force
Tdα	alpha axis disturbance torque
Tdβ	beta axis disturbance torque
l_e	Length of moment arm

LIST OF ABBREVIATIONS

A   Ampere
CAD   Computer Aid Design
DOF   Degree of Freedom
DO   Disturbance Observer
FEM   Finite Elements Method
IC   Integrated Circuit
I-PD   Integral, proportional, differential
LOC   Lab on a chip
LIM   Linear Induction Motor
LCD   Liquid Crystal Display
kg   Kilograms
kN   Kilonewtons
kW   Kilowatts
mm   Millimeters
MAGLEV   Magnetic Levitation
m   Meters
N   Newton
PM   Permanent Magnet
PID   Proportional, integral, differential
SS   State Space
SSI   State Space Integral

LIST OF FIGURES

LIST OF TABLES

ABSTRACT

THE ZERO CONTROL OF LINEAR INDUCTION MOTOR DRIVEN MAGNETIC LEVITATED SUSPENSION

Ahmet Fevzi BOZKURT

Department of Mechatronics Engineering

MSc. Thesis

Adviser: Assist. Prof. Dr. Kadir ERKAN

In view of today's technological trends, transportation of objects, which can be nanometer sized particule transporter or a train with several human inside, requires efficiency, reliability and minimum cost by terms.

In this study, a magnetic levitation type 6 DOF (degree of freedom) conveyage system is proposed. According to previous studies, magnetic levitation systems can be used to achieve high speeds (603 km/h Tokyo). Having the qualities of no mechanical friction, relatively low noise, heat, vibration, high precision and robust drivability, electromagnetic levitation technologies have many advantages thanks to the fact that they can operate free of contact.

The proposed magnetic levitation system has three optimazed hybrid poles with motor coils. Several types are simulated under numerical analysis softwares before the final model and each step improved the system by efficiency, robustness and lower cost.

Hence the magnetic levitation force has nonlinear characteristics, it is required to design an active control algorithm. By the same reason, regular PID controller cannot perform. A different type of PID, which is called I-PD is applied as well as SSI and Zero power control. The zero power control is one of the main advantages of hybrid electromagnetic levitation system. This algorithm uses the position sensors, however the controller's error parameter is current. Since all system can be levitated by only permament magnets force, the algorithm only uses minimal current for stability and according to this, it can be said the system uses zero power to levitate. Zero power controlled system can be driven by

linear motor. The proposed system has reaction plate for both levitation and movement. Reaction plate has iron plate and copper plate, which performs like induction motor core. Motor coils on levitation system moves on reaction plate on both axes, making a planar movement and can be controlled in close loop for precision position control.

In this study, teorical principles described. Modelling and simulation results are given with experimental results.

Key words: Magnetic levitation, hybrid electromagnets, flexible conveyance system, zero power control

ÖZET

DOĞRUSAL ENDÜKSİYON MOTORUYLA TAHRİK EDİLEN MANYETİK YASTIĞIN SIFIR GÜÇ KONTROLÜ

Ahmet Fevzi BOZKURT

Mekatronik Mühendisliği

Yüksek Lisans Tezi

Tez Danışmanı: Yrd. Doç. Dr. Kadir ERKAN

Günümüz teknolojileri, her branşta olduğu gibi ulaşım alanında da nano boyutlardan trenlere kadar en düşük maliyetle en hızlı, kararlı ve verimli sistemler üzerinde çalışmaktadır.

Bu çalışmada 6 serbestlik dereceli esnek bir taşıma sistemi tasarlanmıştır. Yapılan çalışmalara göre manyetik yastıklama teknolojisi ile yüksek hızlara çıkılabilmektedir. Mekanik temasın bulunmadığı bu sistemler sürtünmenin, titreşimin, gürültünün, ısının az olması, kararlı ve hassas olmaları sebebi ile avantajlıdırlar.

Önerilen manyetik yastık, hem bobin hem de motor sargılarını ihtiva etmektedir. Literatür araştırmasında karşılaşılan sistemler ile tasarlanan sistemler, sonlu elemanlar analizi uygulamaları ile irdelenerek farklı tasarımlar üzerinde çalışılmış ve en verimli, kararlı ve daha ucuza üretilebilecek olan son tasarıma ulaşılmıştır.

Manyetik levitasyon sisteminde oluşan kuvvetler ve sistem modellemesi göz önüne alındığında, doğrusal olmayan bir karakteristik ile karşılaşılmaktadır. Ayrıca sistem transfer fonksiyonlarının karakteristiği sebebi ile standart PID kontrolcüsü sistem kararlılığını sağlayamamaktadır. Bu sebeple geliştirilmiş olan I-PD versiyonu, SSI ve sıfır güç kontrol algoritmaları ile birlikte başarı ile uygulanmıştır.Sıfır güç kontrol algoritması, mesafe sensörlerini kullanmasına rağmen akımı değişken olarak kullanarak teoride sıfır akım girişi ile sistemi dengede tutmaktadır. Uygulamalarımızda gürültü ve diğer etkileri bastıran bu kontrölcü neredeyse sıfır akım ise sistemi dengede tutmaktadır.Sıfır güç control algoritması ile havada yastıklanan sistem doğrusal motor ile sürülebilmektedir.

Önerilen sistem reaksiyon plakası üzerinde hem yastıklamayı hem de eksenel hareketleri gerçekleştirebilmektedir. Reaksiyon plakası, endüksiyon motor prensibi ile çalışmakta olup demir ve bakır plakalardan oluşmuştur. Manyetik yastığın üzerindeki motor sargılarının uyartılması ile reaksiyon plakası üzerinde, kapalı çevrim kontrol algoritmaları ile hassas konum kontrol yapılabilmektedir.

Bu çalışmada teorik alt yapı anlatılmakta, modelleme ile benzetim sonuçları, deneysel sonuçlar ile sunulmaktadır.

Anahtar kelimeler: Manyetik yastıklama, hibrit elektromıknatıslar, esnek taşıma sistemleri, sıfır güç kontrol

INTRODUCTION

1.1   Literature Review

Latest technology trends needs precision and reliable robustness for manufacturing and experimental studies. Manufactured item can be several tons to nanometer size. IC, LCD monitors and LOC production needs clean room environment. Clean room applications requires an environment which is vibrate free, heat radiation free and all kinds of noise is unacceptable.

No mechanical friction, heat, vibration and relatively low noise are the qualities of maglev systems to the fact free of contact operate [1-3].

Different types of maglev systems are studied. Using hybrid electromagnets gives opportunity to achieve zero power control [4], however levitating the steel plate requires stationary trust motors and completely passive plate [5,6,7].

Different control algorithms studied, like sliding mode [8,9,10], adaptive control [11], robust control [12-16] and more complex algorithms combined. Another approach is controlling maglev systems with nonlinear model approach which results better real life experiments [17,18,19]. And one of the soft sensor method called disturbance observer [20].

High order controlling methods using artificial intelligent and fuzzy logic can be applied [21,22].

LCD conveyor system has electromagnetic levitation method with guide rollers. Linear induction motor controls the trust force and electromagnets levitates the mover.
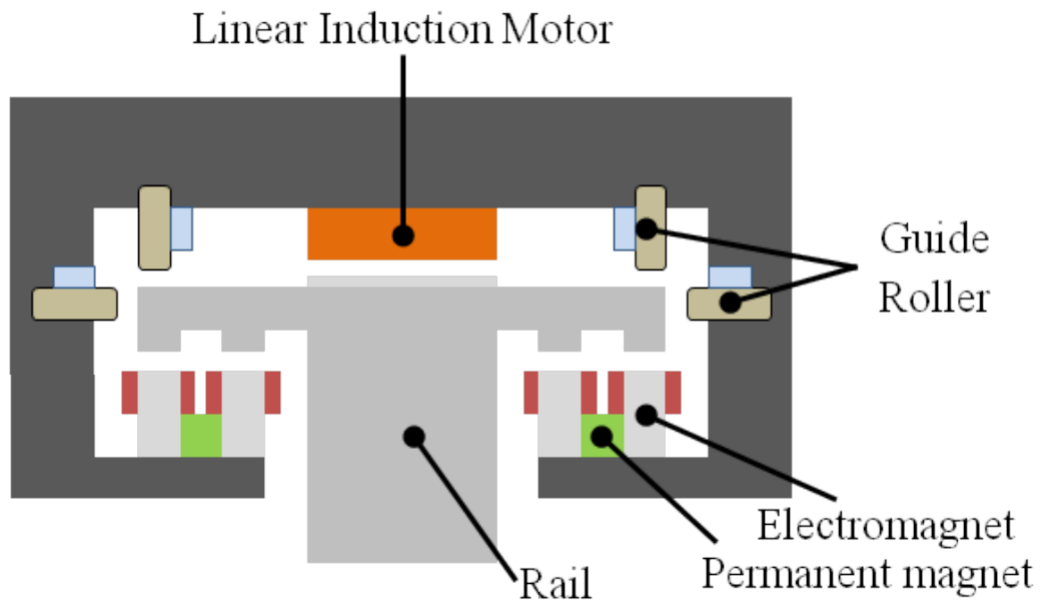
Figure 1.1 LCD conveyor system

Maglev trains have different approaches for levitation and shown in figure 1.2.

Figure 1.2 Levitation techniques

Moreover another indoor application is using four pole hybrid electromagnets for higher efficiency. This method uses permanent magnets and electromagnets combined. The called "zero power control" levitates the system with only permanent magnets and applies very low input signals to control stability.
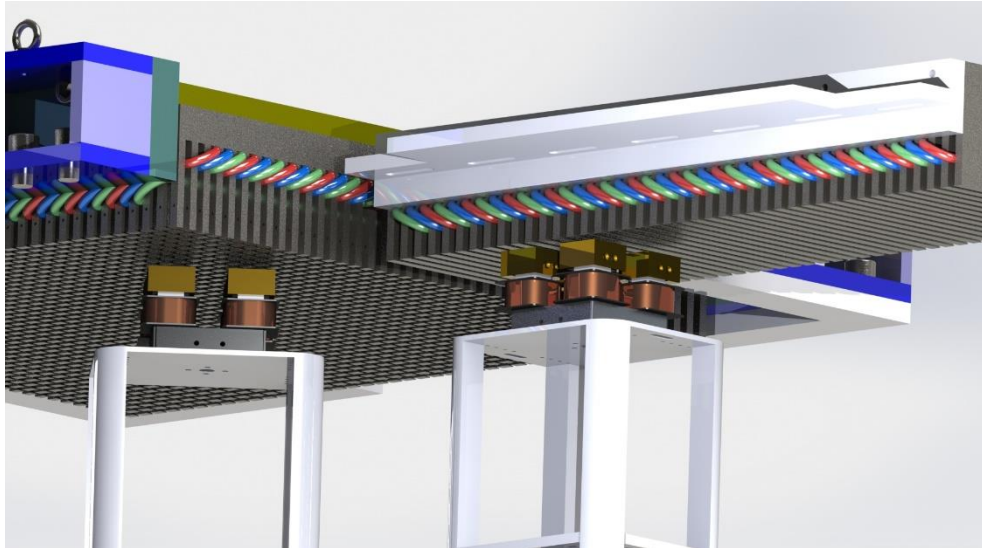
Figure 1.3 Linear and planar motion with hybrid maglev movers

Figure 1.3 shows active rail maglev system. However, linear motors can be on mover and rail can be completely passive. This kind of movers requires better energy source for longer period of work.
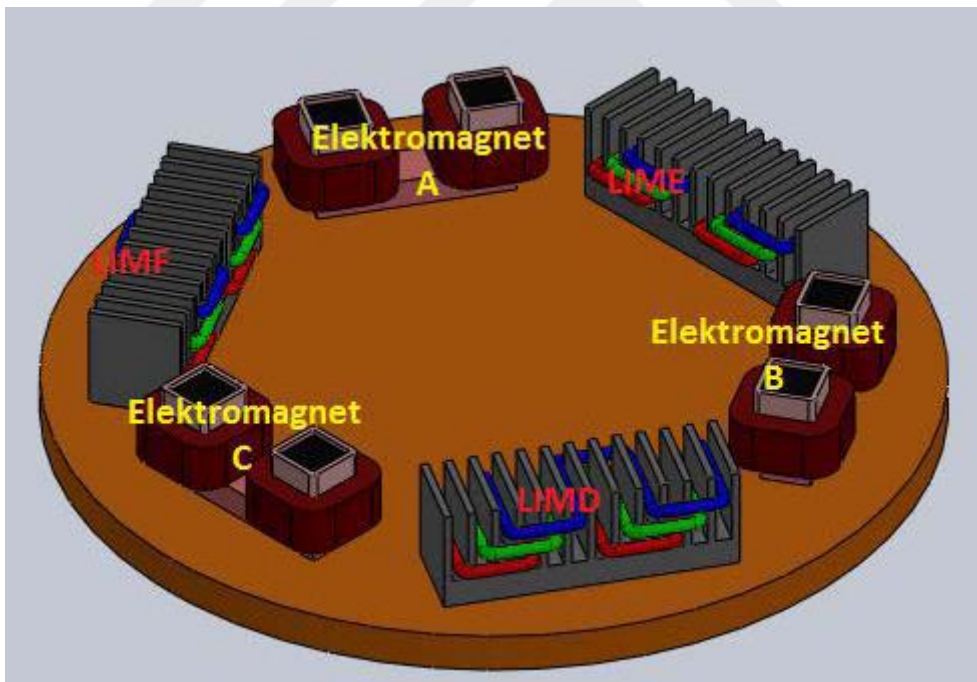
Figure 1.4 Triple U type electromagnet levitation system

1.2 Objective of the Thesis

The aim of the study is designing, manufacturing and controlling of complete maglev conveyor system using different control algorithms.

Design will be patentable. Earlier studies show us a new type hybrid electromagnet can be design and controlled. All analysis and manufacturing process will be done.

Because the system has hybrid electromagnets, the most efficient control algorithms is zero power control method. To simplify the complete system, levitation and driving systems separately modelled and controlled. Zero power control is used for levitation and another algorithm of control is used for linear induction motor motion.

This study will acquire the "know-how" of maglev systems. Also design and manufacture stages will improve designing capabilities and will lead to new designs be done.

1.3   Hypothesis

Using electromagnets with hybrid pole which includes permanent magnets, a maglev system can be levitate using zero power method with very high efficiency. Three hybrid linear motors can be used as induction motor on iron and copper plated passive planar rail system. To achieve this six degree of freedom, linearization can be applied to use lower order control algorithms which increments the speed to experiment. Higher order and more complex control algorithms can be applied, but nonlinear characteristics of maglev system limits compute power by double integral equations. Real time control requires high computer capacity and precise power units.

SYSTEM IDENTIFICATION AND SIMULATIONS

In this chapter, theoretical modelling of 6 DOF combined magnetic levitation motor design is performed. Levitation and linear / planar motion are designed separately. Whole system has 6 degree of freedom;

- Z axis of levitation, which is called as air gap

- Alpha axis rotation, around x axis

- Beta axis rotation, around y axis

- X axis linear movement

- Y axis linear movement

- Theta axis rotation, around z axis

Modelling should be done attentively to correspond to controller requests.

2.1 Modelling of Levitation

Proposed system has three U type unique electromagnets, in this study, a new patent pending design is proposed. This new design has an extended U type magnet core with three-phase motor coils. According to FEM analysis; however, system still has U type electromagnet characteristics. As a result, modelling and simulations will be applied accepting it as a U type electromagnet. Analysis results and improvements of new design with parameters are given in next chapters. Complete system modelling can be done step by step starting from single U type modelling. Free body diagram is given at figure 2.1.
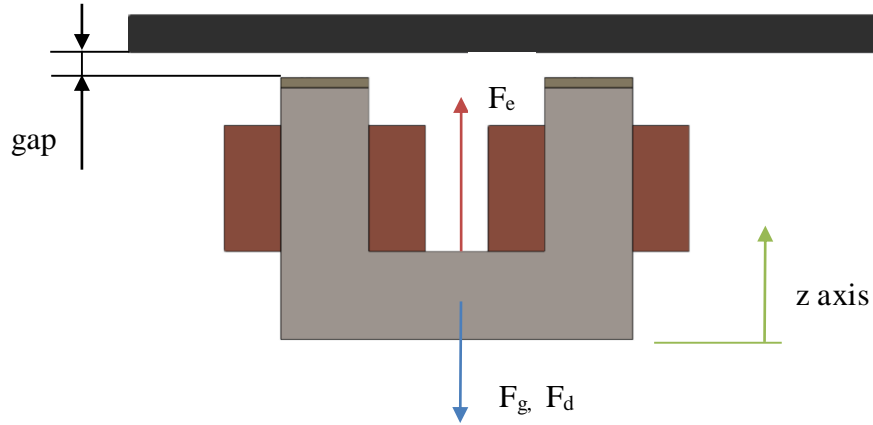
Figure 2.1 Free body diagram of U type hybrid electromagnet

Magnetic force formula can be obtained by solving the equations below;

$$H_m = \frac{B}{\mu} - H_c \ , \quad \mu = \frac{B_r}{H_c} \ , \quad H_g = \frac{B}{\mu_0} \tag{1}$$

$$\oint H dl = N I_f \tag{2}$$

$$B = \frac{Ni + 2H_c L_m}{2x/\mu_0 + 2L_m/\mu} \tag{3}$$

$$F_e = \frac{B^2}{\mu_0} S = \frac{\mu_0 S N^2}{4} \left(\frac{i + 2H_c L_m/N}{x + L_m/\mu_m} \right) \tag{4}$$

$$F_e = k \left(\frac{i + i_m}{x + L_m/\mu_m} \right)^2 \tag{5}$$

$$m\ddot{x} = -F_e + mg + F_d \tag{6}$$

$$m = M/3 \ , \quad x = x_0 + \Delta x \ , \quad i = i_0 + \Delta i \tag{7}$$

Linearization point of (x₀ i₀);

$$m(\ddot{x}_0 + \Delta \ddot{x}) = -k \left(\frac{(i_0 + \Delta i) + i_m}{(x_0 + \Delta x) + L_m/\mu_m} \right)^2 + mg + F_d \tag{8}$$

6

$$m\Delta\ddot{x} = -k\left(\frac{i_0 + i_m}{x_0 + L_m\big/\mu_m}\right)^2 + K_x\Delta x - K_{ix}\Delta i + mg + F_d \qquad (9)$$

If $\Delta\ddot{x}$ obtained from the equation;

$$\Delta\ddot{x} = -\frac{k}{m}\left(\frac{i_0 + i_m}{x_0 + L_m\big/\mu_m}\right)^2 + \frac{K_x}{m}\Delta x - \frac{K_{ix}}{m}\Delta i + g + \frac{F_d}{m} \qquad (10)$$

where;

$$-\frac{k}{m}\left(\frac{i_0 + i_m}{x_0 + L_m\big/\mu_m}\right)^2 = g \qquad (11)$$

Simplified equation is;

$$\Delta\ddot{x} = \frac{K_x}{m}\Delta x - \frac{K_{ix}}{m}\Delta i + \frac{F_d}{m} \qquad (12)$$

For energy efficiency, linearization point should be selected at $i_0 = 0$ levitation point. This point also sets the reference of zero power control algorithm.

Axes transformation equations for triple configuration of electromagnets are given below.

$$M\frac{d^2}{dt^2}\Delta x_{A,B,C} = 3K_x\Delta x_{A,B,C} - 3K_{ix}\Delta i_{A,B,C} + 3F_{d_{A,B,C}} \quad , \quad m^{-1} = \frac{3}{M} \qquad (13)$$

Decentralized design equations of each electromagnets are as follows;

$$\frac{d^2}{dt^2}\Delta x_A = \frac{3}{M}K_x\Delta x_A - \frac{3}{M}K_{ix}\Delta i_A + \frac{3}{M}F_{d_A} \qquad (14)$$

$$\frac{d^2}{dt^2}\Delta x_B = \frac{3}{M}K_x\Delta x_B - \frac{3}{M}K_{ix}\Delta i_B + \frac{3}{M}F_{d_B} \qquad (15)$$

$$\frac{d^2}{dt^2} \Delta x_C = \frac{3}{M} K_x \Delta x_C - \frac{3}{M} K_{ix} \Delta i_C + \frac{3}{M} F_{d_C} \qquad (16)$$

Recalculating the equations with "m" variable;

$$\frac{d^2}{dt^2} \Delta x_A = \frac{1}{m} K_x \Delta x_A - \frac{1}{m} K_{ix} \Delta i_A + \frac{1}{m} F_{d_A} \qquad (17)$$

$$\frac{d^2}{dt^2} \Delta x_B = \frac{1}{m} K_x \Delta x_B - \frac{1}{m} K_{ix} \Delta i_B + \frac{1}{m} F_{d_B} \qquad (18)$$

$$\frac{d^2}{dt^2} \Delta x_C = \frac{1}{m} K_x \Delta x_C - \frac{1}{m} K_{ix} \Delta i_C + \frac{1}{m} F_{d_C} \qquad (19)$$

Final force equations;

$$F = ma; \qquad (20)$$

$$F_{e_A} = -K_x \Delta x_A + K_{ix} \Delta i_A \qquad (21)$$

$$F_{e_B} = -K_x \Delta x_B + K_{ix} \Delta i_B \qquad (22)$$

$$F_{e_C} = -K_x \Delta x_C + K_{ix} \Delta i_C \qquad (23)$$

where;

$$K_x = 2k \frac{\left(i_0 + i_m\right)^2}{\left(x_0 + L_m\right)^3} \qquad (24)$$

$$K_{ix} = 2k \frac{\left(i_0 + i_m\right)}{\left(x_0 + L_m\right)^2} \qquad (25)$$

Simulated system has three identical U type electromagnets hence K_x and K_{ix} parameters are equal for each electromagnet.

Further equations are written for axes transformations. Three electromagnets' gap are combined in equations for z, alpha and beta axes for more responsive control and easier experiments. Axes transformations requires real system sizes. Figure 2.2 shows final design of proposed system which is drawn in CAD program. This approach help to

prevent model errors and system unexpected distortions and simulation parameters will be similar with experimental parameters in this way.
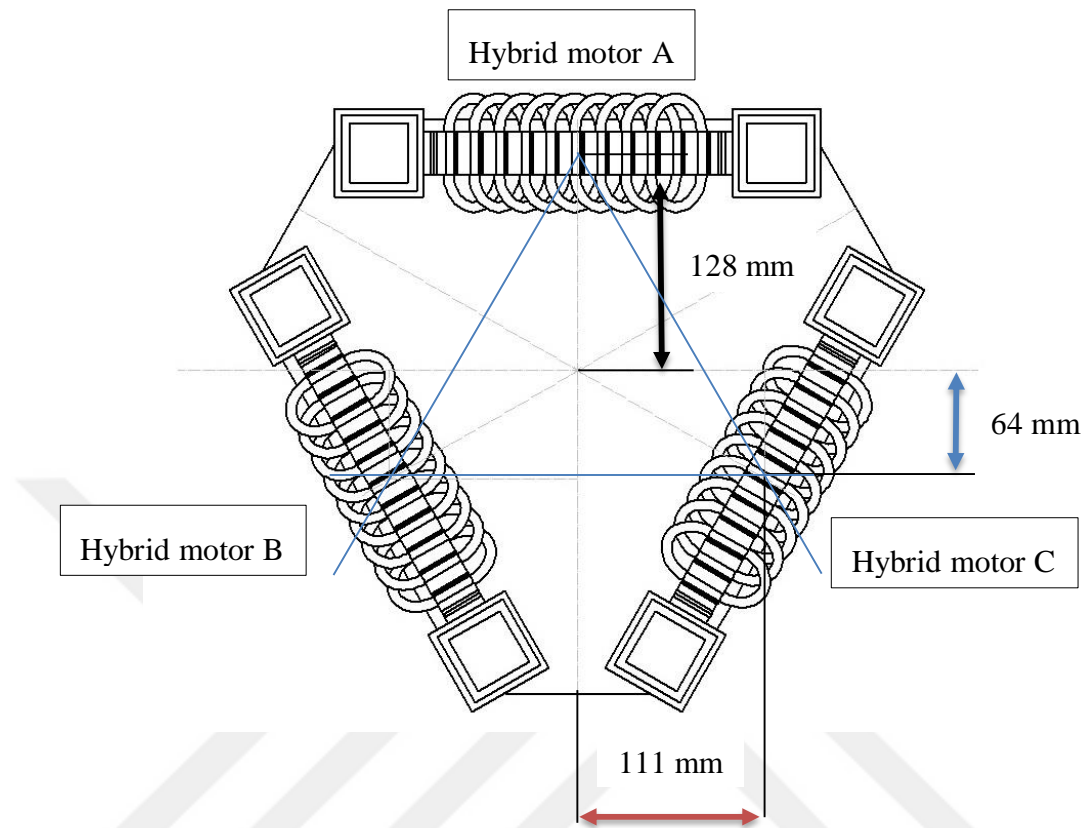
Figure 2.2 Axes transformation and moment arm length for each axis
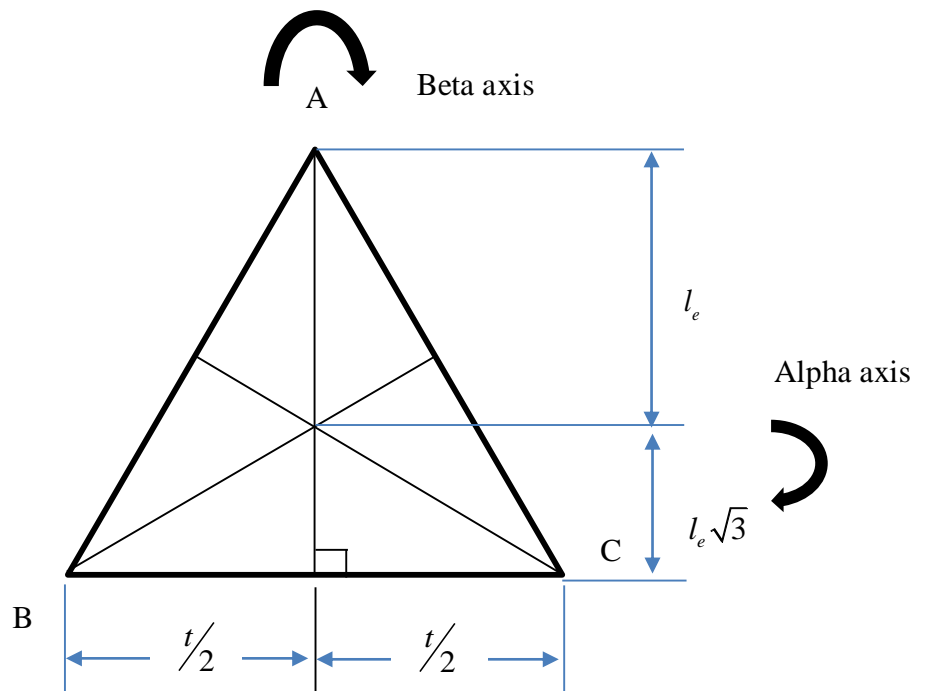
Figure 2.3 Projection force center points and system size parameters

Calculated decentralized formulas will be used to achieve axes formulas. For z axis transformation;

$$M \frac{d^2}{dt^2} z = F_{e_A} + F_{e_B} + F_{e_C} - F_{d_A} - F_{d_B} - F_{d_C} \tag{26}$$

$$M \frac{d^2}{dt^2} z = -K_z \Delta x_A + K_{iz} \Delta i_A - K_z \Delta x_B + K_{iz} \Delta i_B - K_z \Delta x_C + K_{iz} \Delta i_C - F_{d_A} - F_{d_B} - F_{d_C} \tag{27}$$

$$M \frac{d^2}{dt^2} z = -K_z \left(\Delta x_A + \Delta x_B + \Delta x_C \right) + K_{iz} \left(\Delta i_A + \Delta i_B + \Delta i_C \right) - \left(F_{d_A} + F_{d_B} + F_{d_C} \right) \tag{28}$$

Solving the equations for z and i_z and final z axis equations are;

$$\Delta z = -\frac{\Delta x_A + \Delta x_B + \Delta x_C}{3} \tag{29}$$

$$\Delta i_z = \frac{\Delta i_A + \Delta i_B + \Delta i_C}{3} \tag{30}$$

$$F_{d_z} = F_{d_A} + F_{d_B} + F_{d_C} \tag{31}$$

$$M \frac{d^2}{dt^2} z = 3K_z \Delta z + 3K_{iz} \Delta i - F_{d_z} \tag{32}$$

Force triangle is equilateral triangle because of symmetrical design. Considering this, geometrical transformations give us the parameters for alpha and beta axes transformations. "h" is length of triangle and l_e is 2/3 of h. Geometrical parameters are given in figure 2.3 and equations are given below.

$$3l_e = 2h \quad, \quad h = \frac{3}{2} l_e \tag{33}$$

$$t = \frac{\frac{3}{2} l_e}{\cos(30)} \quad, \quad t = l_e \sqrt{3} \quad, \quad \frac{t}{2} = \frac{\sqrt{3}}{2} l_e \tag{34}$$

$$\Delta \alpha = -\left(\Delta x_A - \frac{\Delta x_B + \Delta x_C}{2} \right) \frac{1}{\frac{3l_e}{2}} \tag{35}$$

$$\Delta \beta = \frac{\Delta x_C - \Delta x_B}{t} = \frac{\Delta x_C - \Delta x_B}{l_e \sqrt{3}} \tag{36}$$

After the geometric transformations applied, torque equations are;

$$J_\alpha \frac{d^2}{dt^2}\Delta\alpha = l_e F_{e_A} - {l_e}\big/{2}\left(F_{e_B} + F_{e_C}\right) + \left({l_e}\big/{2}\, F_{d_B} + {l_e}\big/{2}\, F_{d_C} - l_e F_{d_A}\right) \tag{37}$$

$$J_\alpha \frac{d^2}{dt^2}\Delta\alpha = l_e\left(-K_z\Delta x_A + K_{iz}\Delta i_A\right) - {l_e}\big/{2}\left(-K_z\Delta x_B + K_{iz}\Delta i_B - K_z\Delta x_C + K_{iz}\Delta i_C\right) + {l_e}\big/{2}\left(F_{d_B} + F_{d_C} - 2F_{d_A}\right)$$

$$J_\alpha \frac{d^2}{dt^2}\Delta\alpha = \frac{3}{2}l_e^2 K_z\Delta\alpha + l_e K_{iz}\Delta i_\alpha - F_{d_\alpha} \tag{39}$$

Alpha axis variables;

$$\Delta\alpha = \frac{2\Delta x_A}{3l_e} - \frac{\Delta x_B + \Delta x_C}{3l_e} \tag{40}$$

$$\Delta i_\alpha = \Delta i_A - \frac{\Delta i_B - \Delta i_C}{2} \tag{41}$$

$$F_{d_\alpha} = -{l_e}\big/{2}\left(F_{d_B} + F_{d_C} - 2F_{d_A}\right) \tag{42}$$

Beta axis transform equations;

$$J_\beta \frac{d^2}{dt^2}\Delta\beta = l_e\,{\sqrt{3}}\big/{2}\left(F_{e_B} - F_{e_C}\right) - l_e\,{\sqrt{3}}\big/{2}\left(F_{d_B} + F_{d_C}\right) \tag{43}$$

$$J_\beta \frac{d^2}{dt^2}\Delta\beta = l_e\sqrt{{3}\big/{2}}\left(-K_a\Delta g_B + K_b\Delta i_C\right) - l_e\sqrt{{3}\big/{2}}\left(-K_a\Delta g_C + K_b\Delta i_C\right) + l_e\sqrt{{3}\big/{2}}\left(-F_{d_B} + F_{d_C}\right)$$

$$J_\beta \frac{d^2}{dt^2}\Delta\beta = \frac{3}{2}l_e^2 K_a\Delta\beta + l_e K_b\Delta i_\beta - F_{d_\beta} \tag{45}$$

Similar to alpha axis, Beta axis variables;

$$\Delta\beta = \frac{\Delta g_C - \Delta g_B}{l_e\sqrt{3}} \tag{46}$$

$$\Delta i_\beta = \sqrt{3}\,\frac{\Delta i_B - \Delta i_C}{2} \tag{47}$$

$$F_{d_\beta} = l_e\sqrt{{3}\big/{2}}\left(F_{d_C} - F_{d_B}\right) \tag{48}$$

11

After axes transforms, each parameter has written in matrix form.

$$\frac{d}{dx}\begin{bmatrix} \Delta z \\ \Delta \dot{z} \end{bmatrix} = \begin{bmatrix} 0 & 1 \\ 3K_z/M & 0 \end{bmatrix}\begin{bmatrix} \Delta z \\ \Delta \dot{z} \end{bmatrix} + \begin{bmatrix} 0 \\ 3K_{iz}/M \end{bmatrix}\Delta i_z + \begin{bmatrix} 0 \\ -1/M \end{bmatrix}F_{d_z} \tag{49}$$

$$\frac{d}{dx}\begin{bmatrix} \Delta \alpha \\ \Delta \dot{\alpha} \end{bmatrix} = \begin{bmatrix} 0 & 1 \\ \dfrac{3l_e^2}{2}\dfrac{K_z}{J_\alpha} & 0 \end{bmatrix}\begin{bmatrix} \Delta \alpha \\ \Delta \dot{\alpha} \end{bmatrix} + \begin{bmatrix} 0 \\ l_e K_{iz}/J_\alpha \end{bmatrix}\Delta i_\alpha + \begin{bmatrix} 0 \\ -1/J_\alpha \end{bmatrix}F_{d_\alpha} \tag{50}$$

$$\frac{d}{dx}\begin{bmatrix} \Delta \beta \\ \Delta \dot{\beta} \end{bmatrix} = \begin{bmatrix} 0 & 1 \\ \dfrac{3l_e^2}{2}\dfrac{K_z}{J_\beta} & 0 \end{bmatrix}\begin{bmatrix} \Delta \beta \\ \Delta \dot{\beta} \end{bmatrix} + \begin{bmatrix} 0 \\ l_e K_{iz}/J_\beta \end{bmatrix}\Delta i_\beta + \begin{bmatrix} 0 \\ -1/J_\beta \end{bmatrix}F_{d_\beta} \tag{51}$$

Z axis's K_z coefficient can be transform to $K_a = K_z\, l_e$.

Z, alpha and beta axis current and air gap transforms;

$$\begin{bmatrix} \Delta i_z \\ \Delta i_\alpha \\ \Delta i_\beta \end{bmatrix} = \begin{bmatrix} 1/3 & 1/3 & 1/3 \\ 1 & -1/2 & -1/2 \\ 0 & \sqrt{3}/2 & -\sqrt{3}/2 \end{bmatrix}\begin{bmatrix} \Delta i_A \\ \Delta i_B \\ \Delta i_C \end{bmatrix} \tag{52}$$

$$\begin{bmatrix} \Delta z \\ \Delta \alpha \\ \Delta \beta \end{bmatrix} = \begin{bmatrix} -1/3 & -1/3 & -1/3 \\ -2/3l_e & 1/3l_e & 1/3l_e \\ 0 & -1/\sqrt{3}l_e & 1/\sqrt{3}l_e \end{bmatrix}\begin{bmatrix} \Delta x_A \\ \Delta x_B \\ \Delta x_C \end{bmatrix} \tag{53}$$

These equations are for current type controller design, which eliminates the resistance and inductance effects on output. However, in this study voltage driven input will be used. Because of this, electrical dynamics will be added to equations.

$$e(t) = R_z i_z(t) + N\frac{d\Phi}{dx} \tag{54}$$

$$e(t) = R_z i_z(t) + \mu_0 NS \frac{d}{dx}\frac{Ni_z(t)+E_{PM}}{z(t)+I_{PM}} \tag{55}$$

Linearization of the equation above;

$$e(t) = R_z \Delta i_z(t) + L_z \Delta i_z(t) + \frac{K_z L_z}{K_{iz}} \Delta \dot{z}(t) \qquad (56)$$

Laplace transformation applied equation is;

$$I_z(s) = \frac{1}{L_z s - R_z} \left[E_z(s) - \frac{K_z L_Z}{K_{iz}} sZ(s) \right] \qquad (57)$$

Linearized block diagram has been written in MATLAB Simulink program. Hence only coefficients change, angular displacement diagrams has not given.
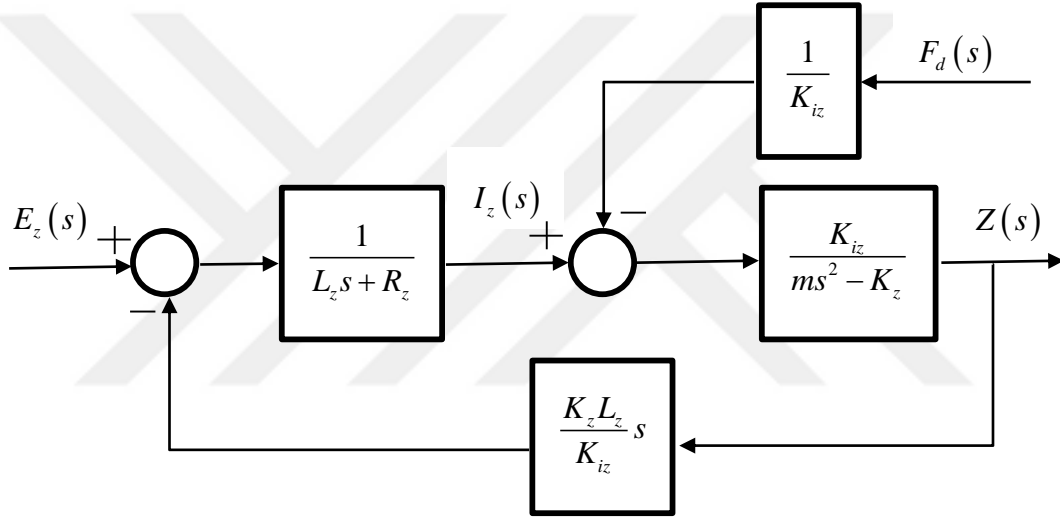
Figure 2.4 System linearized transfer function of Z axis

States of state-space $\Delta z(t)$, $\Delta \dot{z}(t)$ and $\Delta i_z(t)$ can be written in matrix format as;

$$\frac{d}{dt} \begin{bmatrix} \Delta z(t) \\ \Delta \dot{z}(t) \\ \Delta i_z(t) \end{bmatrix} = \begin{bmatrix} 0 & 1 & 0 \\ K_z/m & 0 & K_{iz}/m \\ 0 & -K_x/K_{iz} & -R_z/L_z \end{bmatrix} \begin{bmatrix} \Delta z(t) \\ \Delta \dot{z}(t) \\ \Delta i_z(t) \end{bmatrix} + \begin{bmatrix} 0 \\ 0 \\ 1/L_z \end{bmatrix} \Delta e_z(t) + \begin{bmatrix} 0 \\ -1/m \\ 0 \end{bmatrix} F_d(t) \quad (58)$$

2.1.1 I-PD Controller Design

After obtaining required equations, canonical form representations used for system identification. MATLAB has built-in functions for canonical solver, which is the reason

to choose this method. Linear model and controller, transfer functions and matrices are given below.

$$TF = -\frac{K_{iz}}{\left(LMs^3 + MRs^2 - K_z R\right)}$$ (59)

Controller added closed loop transfer function;

$$TF_{I-PD} = -\frac{K_z K_{iz}}{LMs^4 + MRs^3 + K_d K_{iz}s^2 + (K_{iz}K_p - K_z R)s + K_i K_{iz}}$$ (60)

System is fourth order polynomial as seen from the transfer function and has no zeros. However regular PID controller closed loop has two zeros.

PID controller transfer function is;

$$TF_{PID} = -\frac{K_{iz}K_d s^2 + K_{iz}K_p s + K_i K_{iz}}{LMs^4 + MRs^3 + K_d K_{iz}s^2 + (K_{iz}K_p - K_z R)s + K_i K_{iz}}$$ (61)

Pole-zero map gives characteristic of the system. Both PID and I-PD maps are given in figure 2.5. Since the roots of transfer functions are same, controller parameters are same for both. However, the zero near origin may cause unwanted occasions.
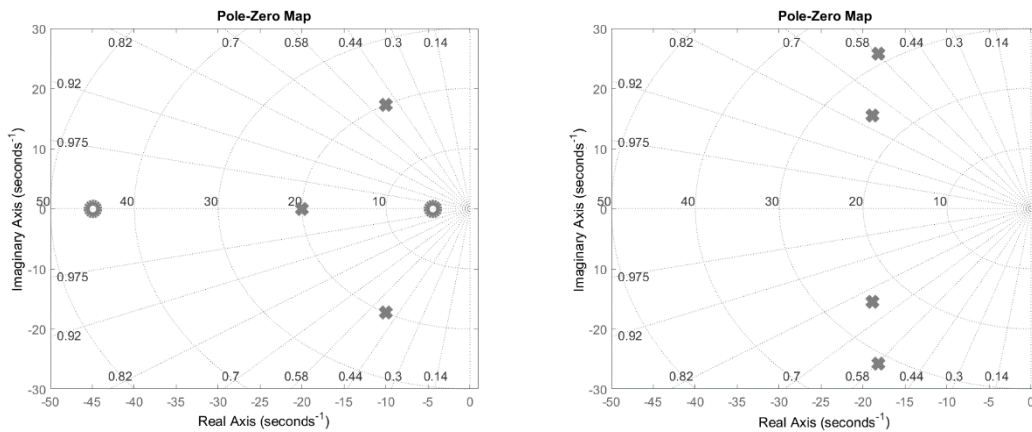
Figure 2.5 Pole-zero maps of PID (left) and I-PD (right) controllers
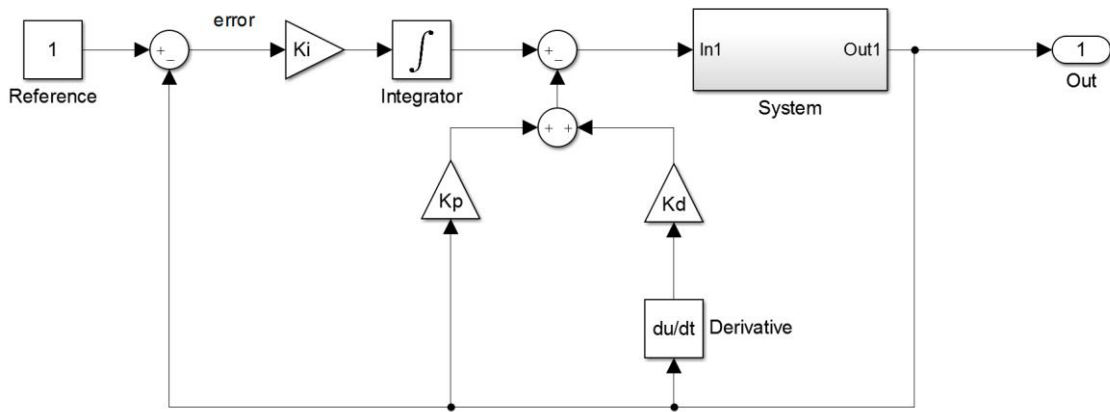
Figure 2.6 I-PD block diagram
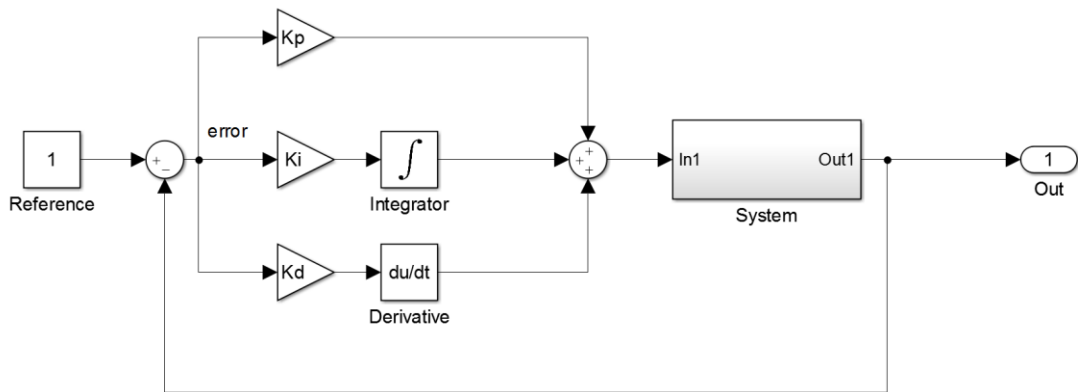
Figure 2.7 PID block diagram

Canonical form can be applied in several modes. Equivalent time constant (τ / tau) can be calculated with stability indexes ($\gamma_{1,2,3,..}$ / gamma$_{1,2,3..}$) or given as an parameter. Canonical form has n-1 γ stability indexes. First, transfer function and canonical polynomial coefficients matching applied.

Canonical form;

$$\frac{Y(s)}{U(s)} = G(s) = \frac{b_2 s^2 + b_1 s + b_0}{a_4 s^4 + a_3 s^3 + a_2 s^2 + a_1 s + a_0} \tag{62}$$

$$\gamma_i = \frac{a_i^2}{a_{i+1} a_{i-1}} \tag{63}$$

$$\tau = \frac{a_1}{a_0} \tag{64}$$

$$a_0 = K_i K_{iz} \,,\ a_1 = K_{iz} K_p - K_z R \,,\ a_2 = K_d K_{iz} \,,\ a_3 = MR \,,\ a_4 = LM \tag{65}$$

Controller parameters calculating tau from its formula are given.

$$K_d = \frac{MR^2}{K_{iz} L \gamma_3} \tag{66}$$

$$K_i = \frac{MR^4}{K_{iz} L^3 \gamma_1 \gamma_2^{\,2} \gamma_3^{\,3}} \tag{67}$$

$$K_p = \frac{MR^3 + K_z L^2 \gamma_2 \gamma_3^{\,2}}{K_{iz} L^2 \gamma_2 \gamma_3} \tag{68}$$

$$\tau = \frac{L \gamma_1 \gamma_2 \gamma_3}{R} \tag{69}$$

Another method is using tau as a parameter and calculating controller with selected tau. This experiment gives opportunity to observe time constant's effect on control.

$$K_d = \frac{MR \gamma_1 \gamma_2}{K_{iz} \tau} \tag{70}$$

$$K_i = \frac{MR \gamma_1^{\,2} \gamma_2}{K_{iz} \tau^3} \tag{71}$$

$$K_p = \frac{MR \gamma_1^{\,2} \gamma_2 + K_z R \tau^2}{K_{iz} \tau^2} \tag{72}$$

Because both PID and I-PD have the same denominator from transfer functions, controller parameters are equal.

In 1960's, Kessler recommends to take all stability indexes 2. However, Manabe in 1980's recommends to take all indexes 2 but γ_1 2,5. These parameters are selected for both simulation and experiments.

Controller parameters are given for calculated tau and parameter tau.

Tau calculated;	Tau given;
tau = 1,077e-01	tau = 1,077e-01
Kp = 1,641e+04	Kp = 1,031e+04
Kd = 2,052e+02	Kd = 2,052e+02
Ki = 3,539e+04	Ki = 3,538e+04

Integral and derivative coefficients are identical for both calculation algorithms when the tau parameter is set to calculated one. However proportional coefficient does differ. Selecting tau and calculating controller parameters gives better response and stability than using tau formula. Other simulations will be done with tau selecting method. First simulation shows the difference between PID and I-PD controllers.

At start, system has negative gap initial value. 0,3 seconds later system reaches steady state and at 0,5 seconds 1mm reference is set and reset at 1,5 seconds. Latest at 2,5 seconds 10N disturbance is applied.

Figure 2.10 shows both controllers give same response to force disturbances. However reference input cause overshoot at PID controller. The zero near origin causes derivate kick for input and result is unacceptable overshoot.

System dynamics are not linear and nonlinear modelling should be applied to maximize similarity between simulation and experimental results. Also all axes should be controlled to maintain stability of 3 DOF levitation system. In decentralized control approach method each magnet controls separately. However, if several axis transforms be applied, total system control can be achieved with centralized control method. Both methods can be used but centralized control calculates the effect of other magnets to one and each, which increases robustness of system. Block diagram and simulation results are given.
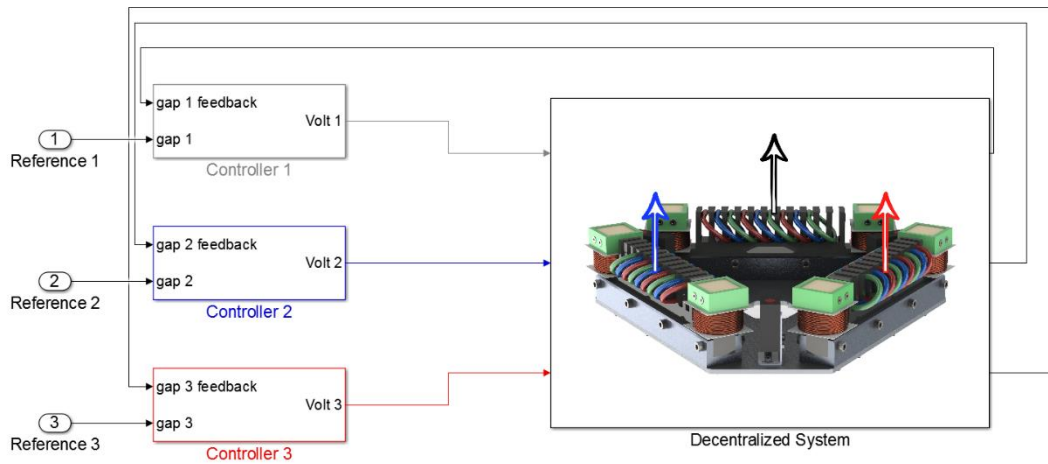
Figure 2.8 Decentralized control block diagram
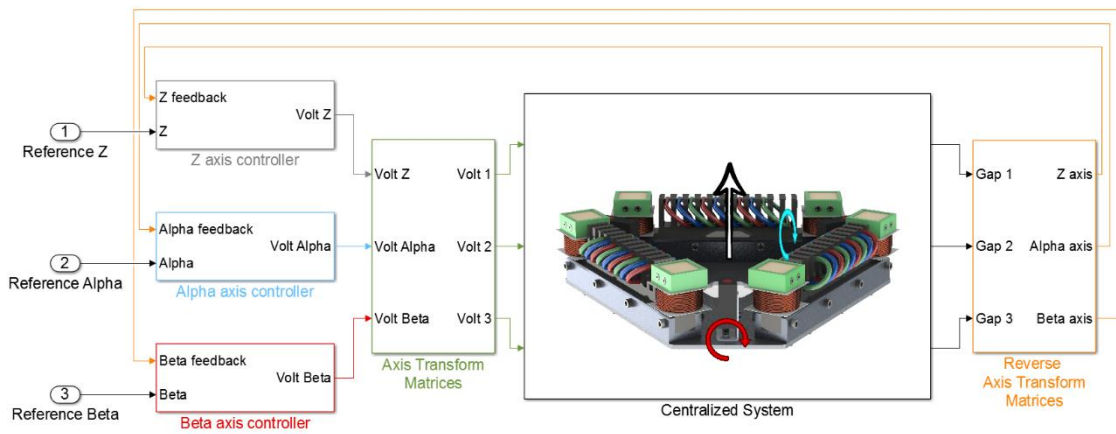
Figure 2.9 Centralized control block diagram
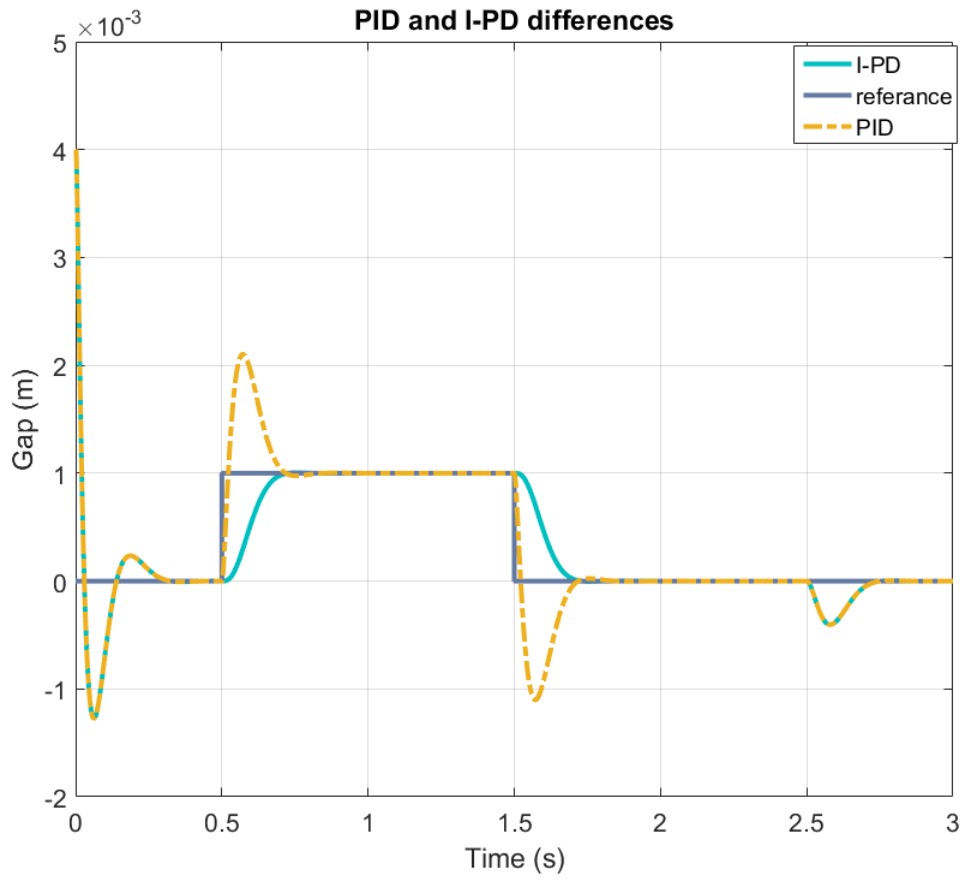
Figure 2.10 PID and I-PD controller compare
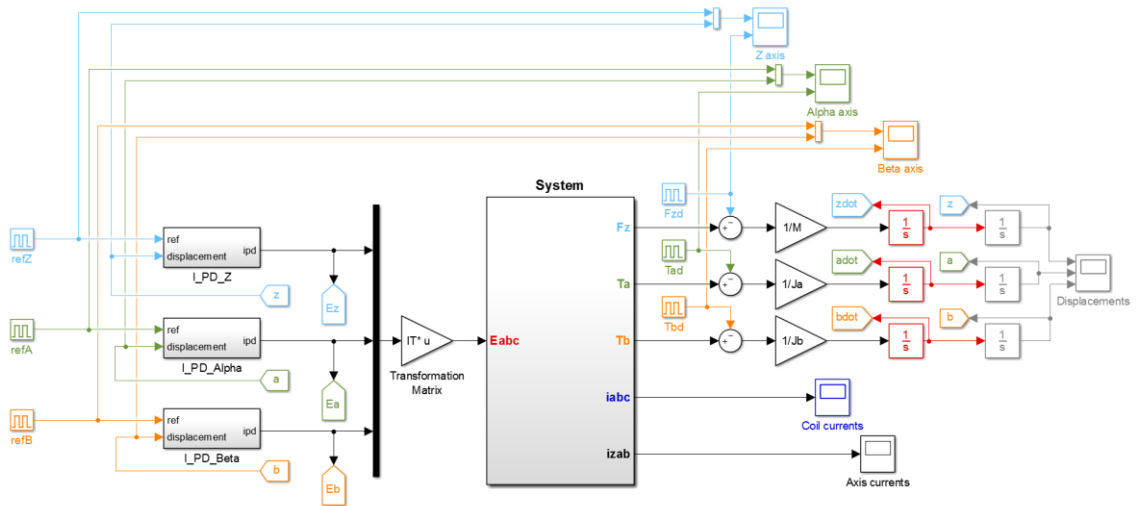
Figure 2.11 3 DOF I-PD controller block diagram
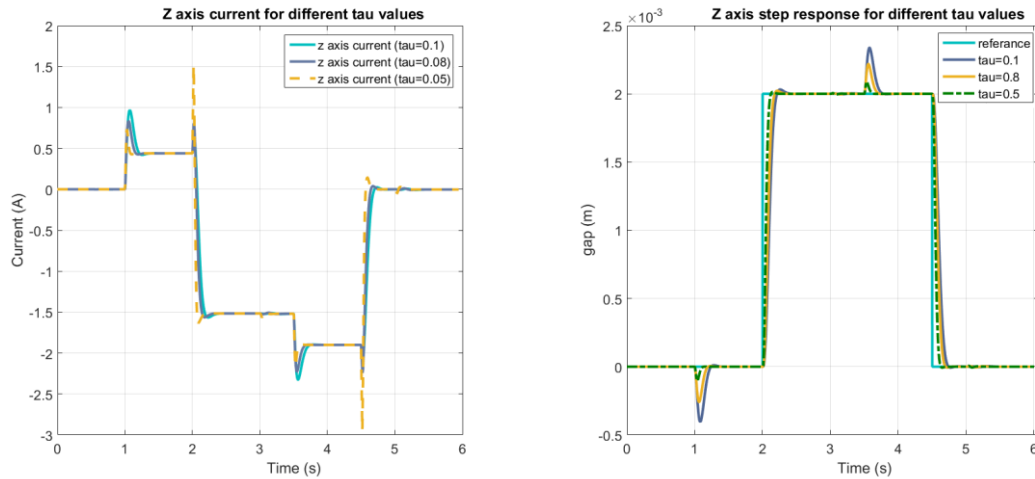
Figure 2.12 Z axis simulation results for different tau values

Figure 2.12 shows higher tau value makes system slower, which lowers the required current input. Simulating system tau=0,05 gives best performance with high capacity of disturbance rejection but currents exceed 3 ampere. This simulation shows higher tau has capability of disturbance rejection with lower current values because of faster response, but reference input cause much higher current in terms. Current should be limited to experiments system limits and tau should be selected feasible. Very low (0.02) tau values cannot be perform experimentally because of system nonlinearity and limits. Proposed system levitated with 0,08 and 0,1 tau and 0,1 gave best performance. All simulations done with 0,1 tau for comparability.

Figure 2.13 Z axis response for reference input and disturbance

Figure 2.14 Alpha and beta axes response for reference input and disturbance
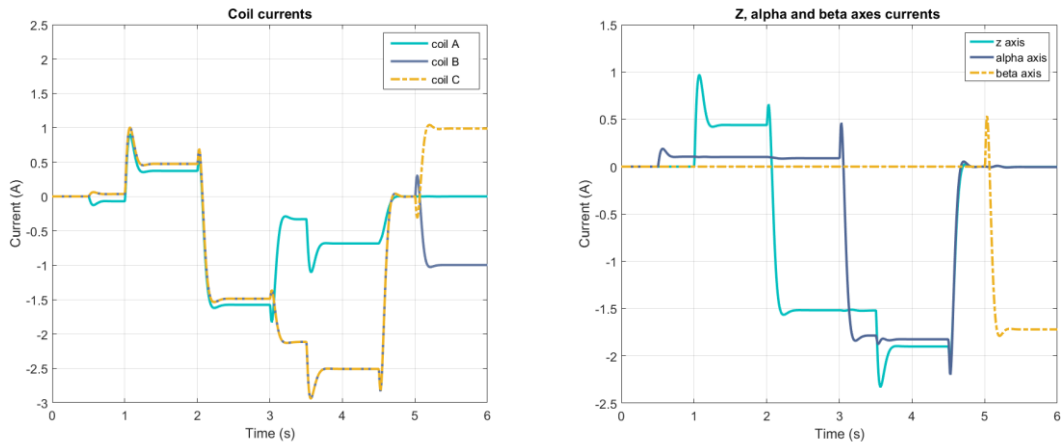
Figure 2.15 Coil and axes currents of simulation

2.1.2 SSI Controller Design

Another approach to control unstable system is SSI control method. State space representation modelling can be applied to obtain states controller needs. A matrices give the poles of system's transfer function. To stabilize system and control, pole placement should be done and system poles should be taken to controllable region.

Main control algorithm is given in figure 2.16. Regular SS controller can levitate the system however controller would not perform well when face a disturbance. SS controller does not promise to cancel out steady state error. Because of this SSI controller should be applied.
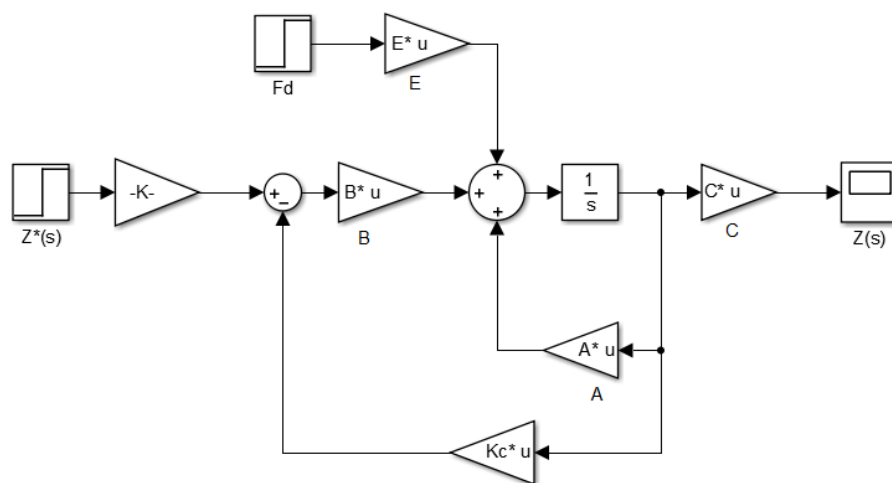
Figure 2.16 State Space controller block diagram

22
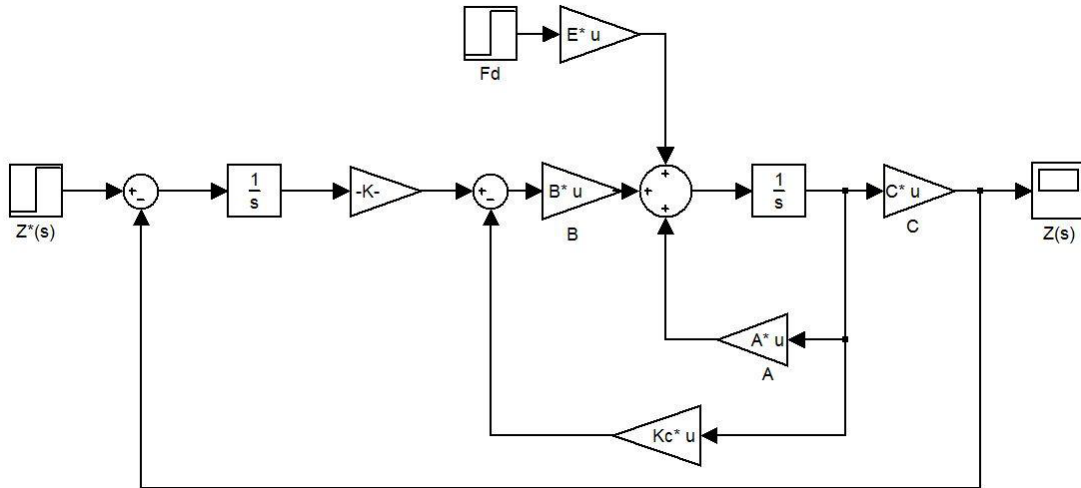
Figure 2.17 State Space Integral controller block diagram

Similar to I-PD controller, SSI controller should be added to all axis to maximize performance. Decentralized control algorithm can be applied but inertia effects shouldn't be forsaken.
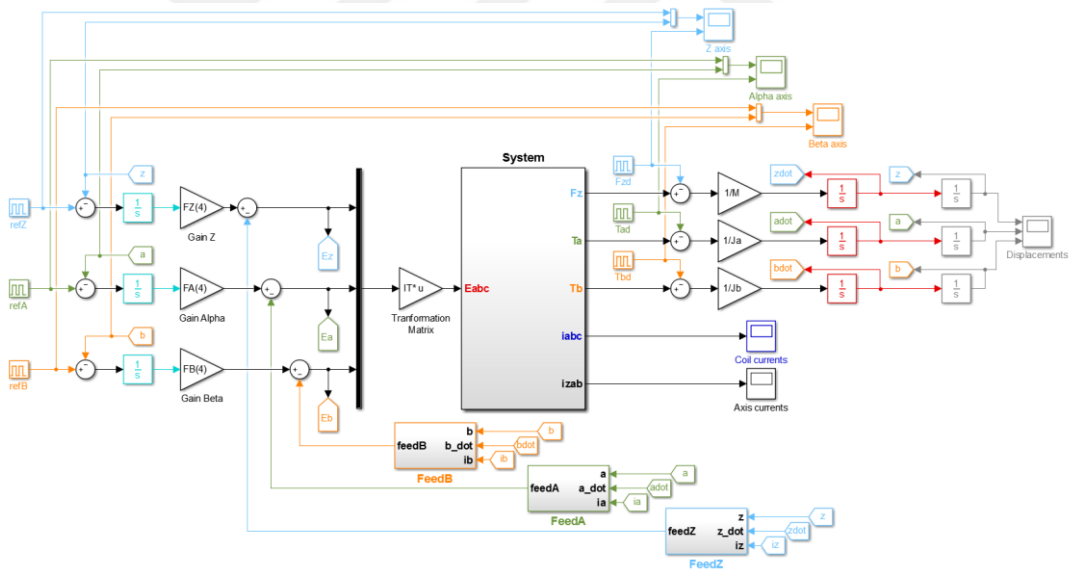
Figure 2.18 3 DOF SSI controller block diagram

Same simulation setup applied to system for comparable results. Controller parameters found with Canonical Polynomial method with Manabe modification. Tau is selected 0,1 as same.
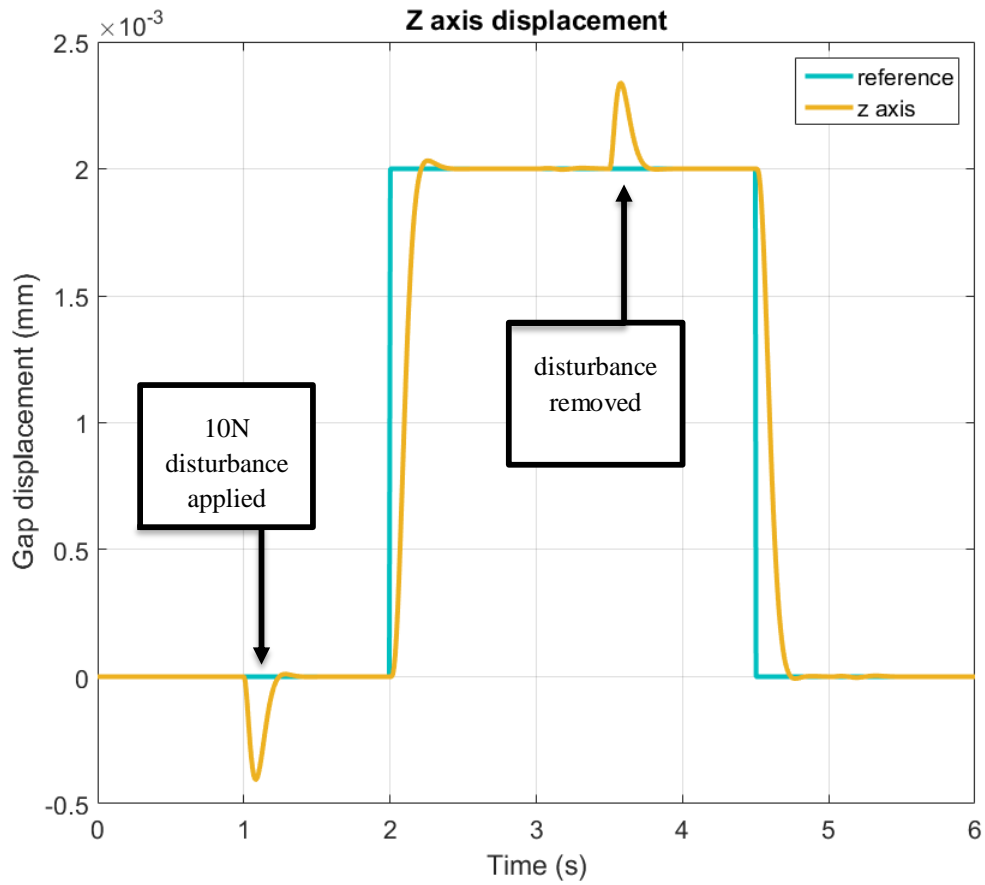
23

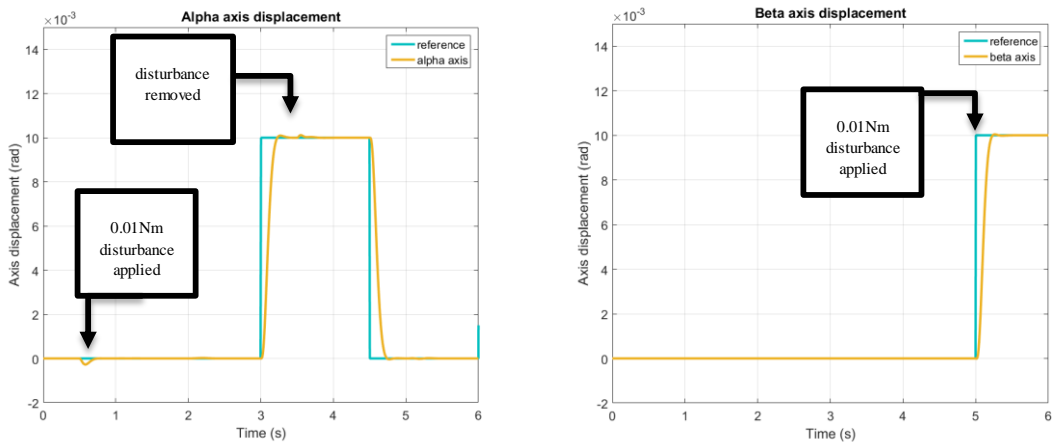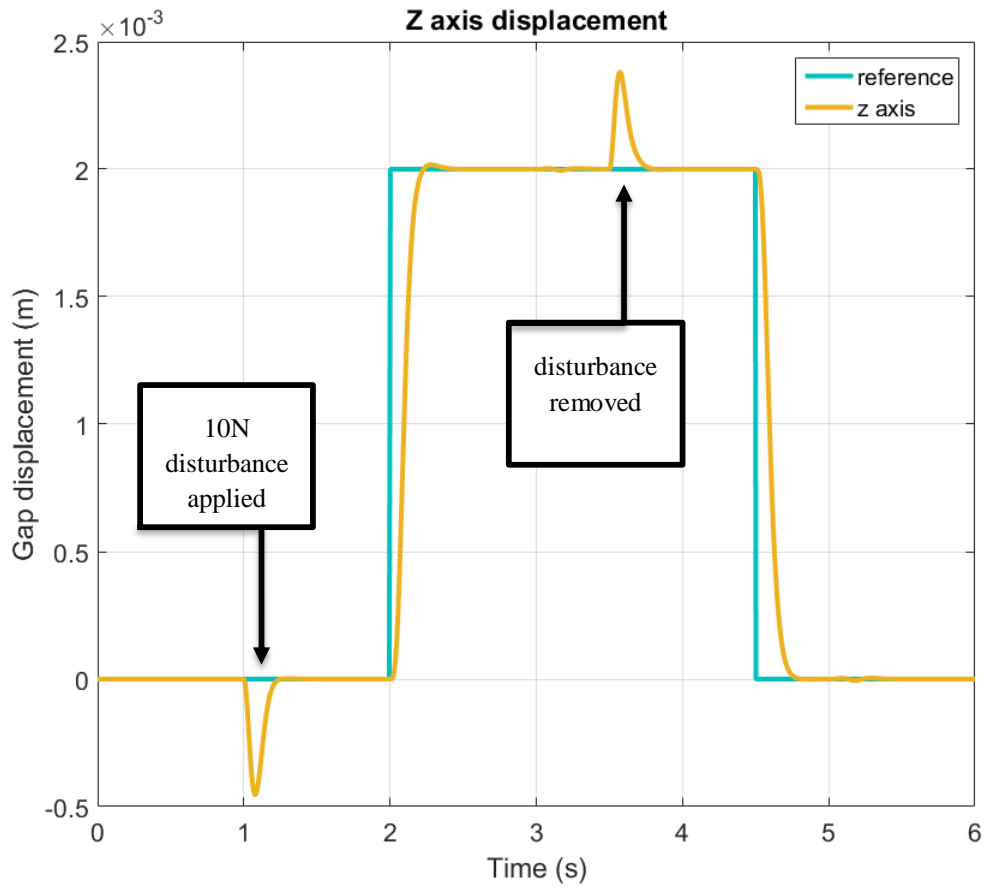Figure 2.19 Z axis response for reference input and disturbance
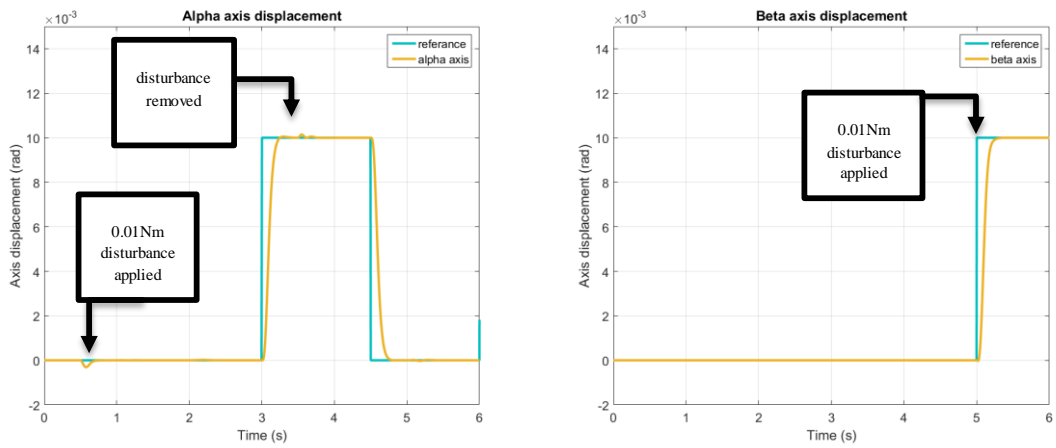
Figure 2.20 Alpha and beta axes response for reference input and disturbance

24
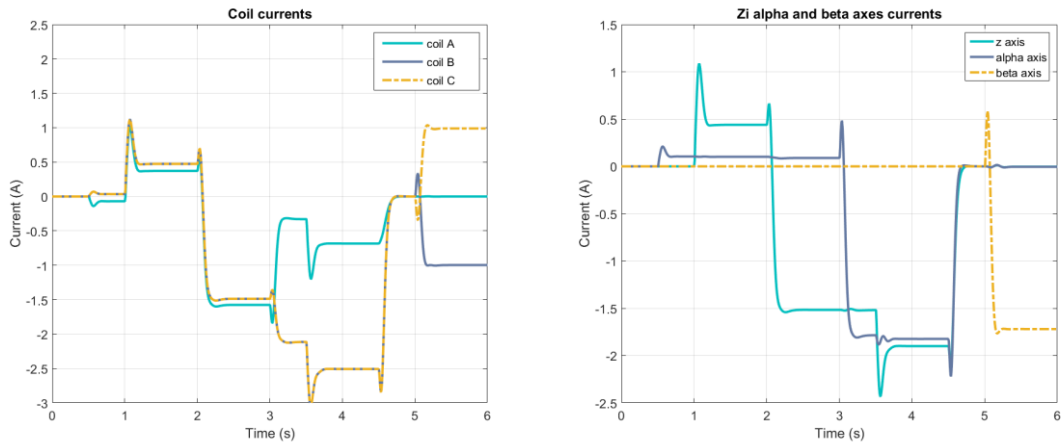
Figure 2.21 Coil and axes currents of simulation

2.1.3 Zero Power Controller Design

Main idea of zero power controller is using voltage as input, and set the reference to 0V. Algorithm is similar to SSI but error calculation feedback taken from voltage.

This simulation has only Z axis disturbance. For robustness, all axes should be controlled separately. To achieve this robustness, all axis have their own zero power controller.
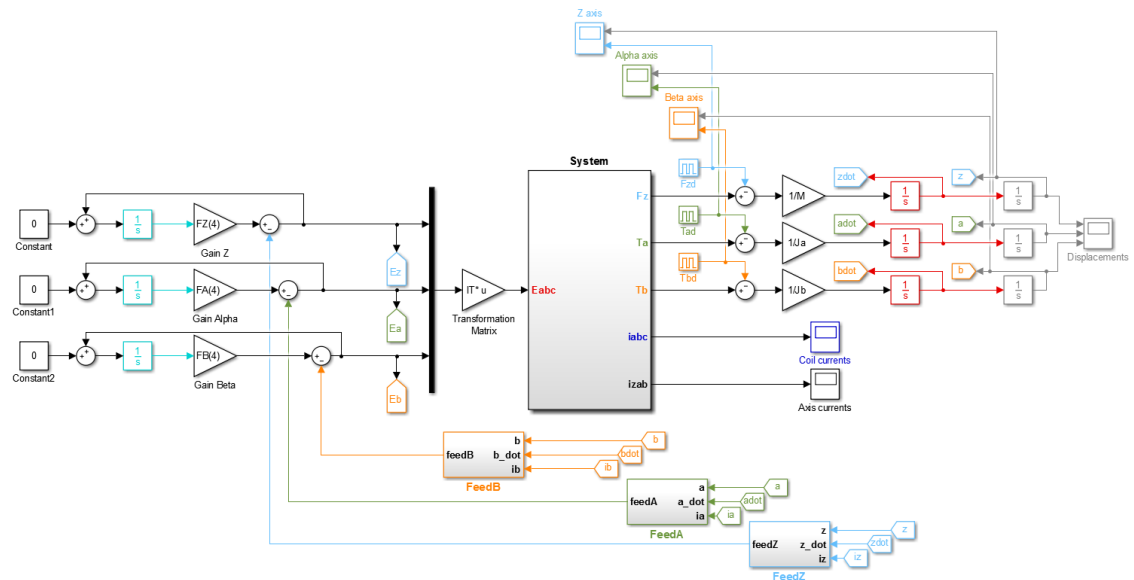
Figure 2.22 3 DOF zero power controller system simulation setup

Gap and magnetic force are inversely proportional which has been proved with FEM analysis. Zero power controller adjusts the gap for achieve zero voltage error. Positive disturbance will decrease the gap to increase attraction force to settle voltage at zero.
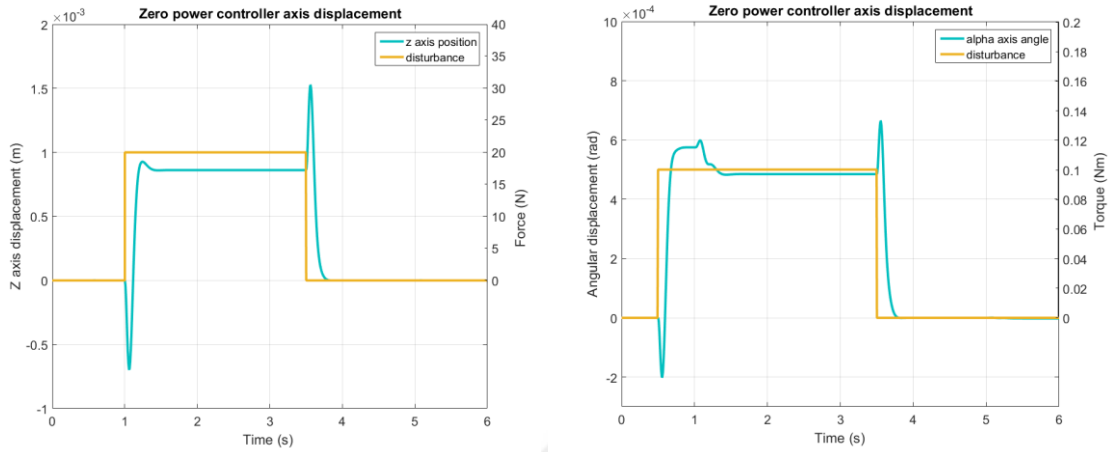
Figure 2.23 Zero power controller axes responses
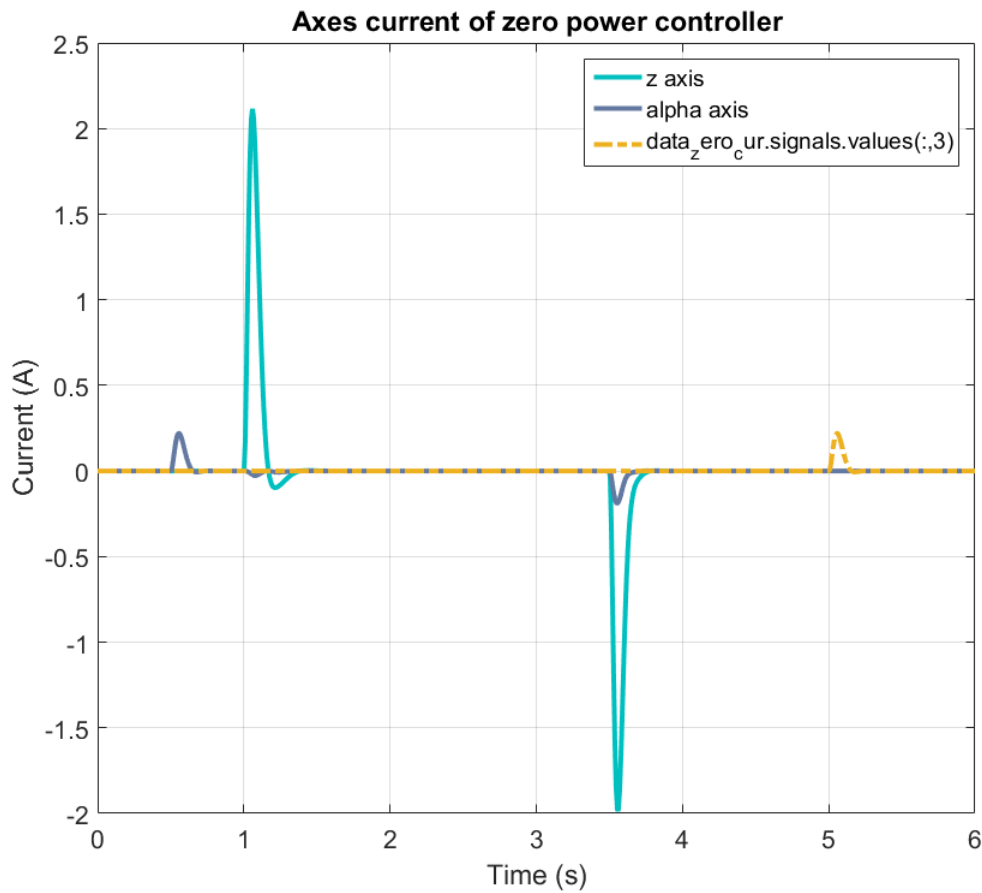
Figure 2.24 Zero power controller axes currents

As seem from figure 2.24, after the transient region passes current converge to zero. Controller overcome current needs with gap adjustment, which can be seen from figure 2.23.

2.1.4 Disturbance Observer Design

Disturbance observer (D.O.) is an S.S. model of system. D.O. predicts the states from inputs and feeds the states to controller as input. It can be perceived of a simulation running beside.

Main advantage of D.O. is that it works as a software sensor network. With predicted velocity and current values, 2 less sensors on each axis will be used and still system can be controlled full of its states.

System must be controllable and observable for D.O. design. And D.O. should be faster than plant because it has to act faster and calculate all required states before a loss. It is recommended to assign D.O. poles to be 2 to 5 times faster than controllers.

Performance of D.O. can be seen simulating the system with and without it. Figure 2.25 shows D.O. well predicts the states and simulation results are similar.
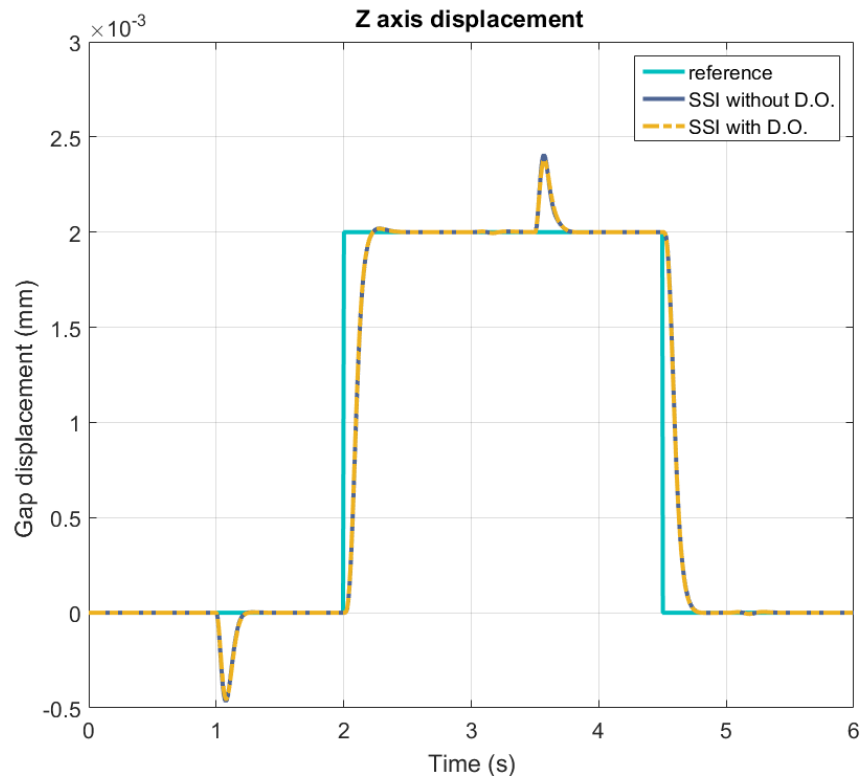
Figure 2.25 Step response of SSI controller with and without D.O

27
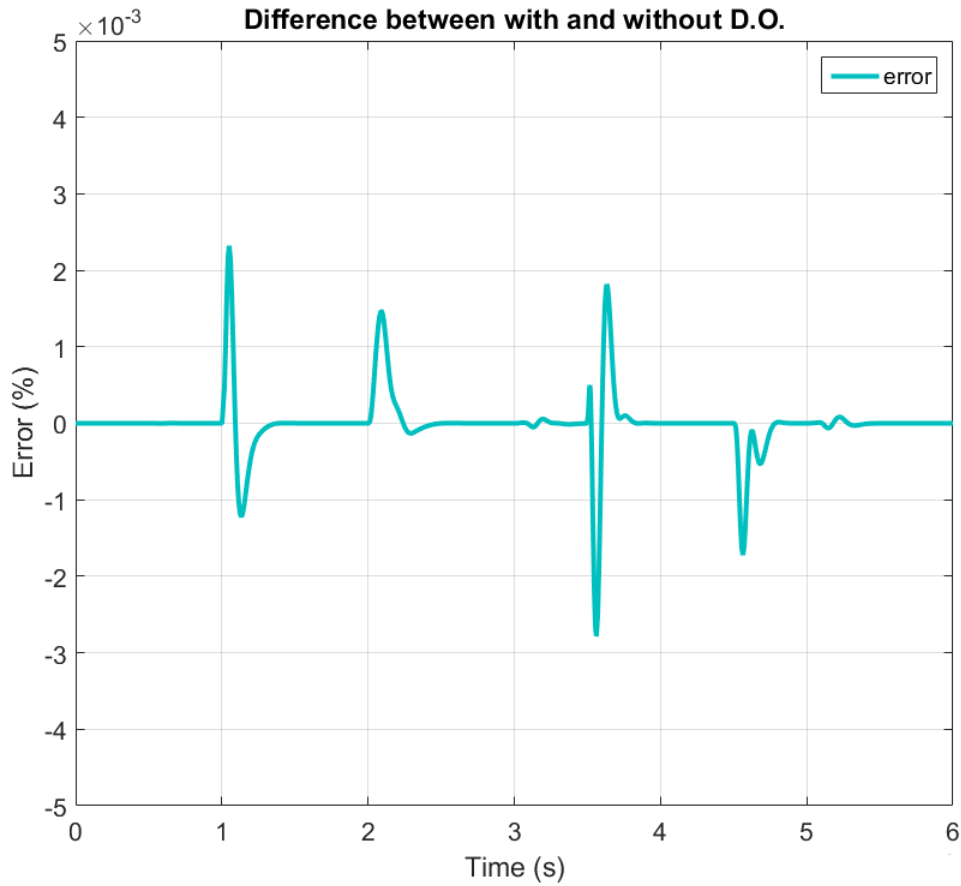
Figure 2.26 Error of disturbance observer

Disturbance observer predicts the disturbances. Disturbance compensation is the most important benefit among the other advantages of this observer. Normally there is no disturbance state in state space representation of plant, however with D.O. a new state is added and an extended matrices is created.

$$\frac{d}{dt}\begin{bmatrix} \Delta z(t) \\ \Delta \dot{z}(t) \\ \Delta i_z(t) \\ F_d \end{bmatrix} = \begin{bmatrix} 0 & 1 & 0 & 0 \\ K_z/m & 0 & K_{iz}/m & -1/m \\ 0 & -K_x/K_{iz} & -R_z/L_z & 0 \\ 0 & 0 & 0 & 0 \end{bmatrix} \begin{bmatrix} \Delta z(t) \\ \Delta \dot{z}(t) \\ \Delta i_z(t) \\ F_d \end{bmatrix} + \begin{bmatrix} 0 \\ 0 \\ 1/L_z \\ 0 \end{bmatrix} \Delta e_z(t)$$

$$\hat{y} = \begin{bmatrix} C & 0 \end{bmatrix}\hat{x} = \begin{bmatrix} 1 & 0 & 0 & 0 \end{bmatrix}\hat{x}$$

System is stable at infinite;

$$t=\infty \quad \Delta z(\infty)=0 \quad \Delta \dot{z}(\infty)=0$$

28

$$0 = \begin{bmatrix} 0 & 1 & 0 \\ K_z/m & 0 & K_{iz}/m \\ 0 & -K_z/K_{iz} & -R_z/L_z \end{bmatrix} \begin{bmatrix} \Delta z(\infty) \\ \Delta \dot{z}(\infty) \\ \Delta i_z(\infty) \end{bmatrix} + \begin{bmatrix} 0 \\ 0 \\ 1/L_z \end{bmatrix} \Delta e_z(\infty) + \begin{bmatrix} 0 \\ -1/m \\ 0 \end{bmatrix} F_d \tag{73}$$

Reorganized equations are given. Disturbance compensation can be calculated solving the equations.

$$\frac{K_{iz}}{m} \Delta i_z(t) - \frac{1}{m} F_d = 0 \tag{74}$$

$$-\frac{R_z}{L_z} \Delta i_z(\infty) + \frac{1}{L_z} \Delta e_z(\infty) = 0 \tag{75}$$

$$K_{Fd} = \frac{\Delta e_z(\infty)}{F_d} = \frac{R_z}{K_{iz}} \tag{76}$$

Output F_d of D.O. multiplied with K_{Fd} and added to control algorithm to increase the disturbance rejection. Disturbance compensation added block diagram is given in figure 2.27.
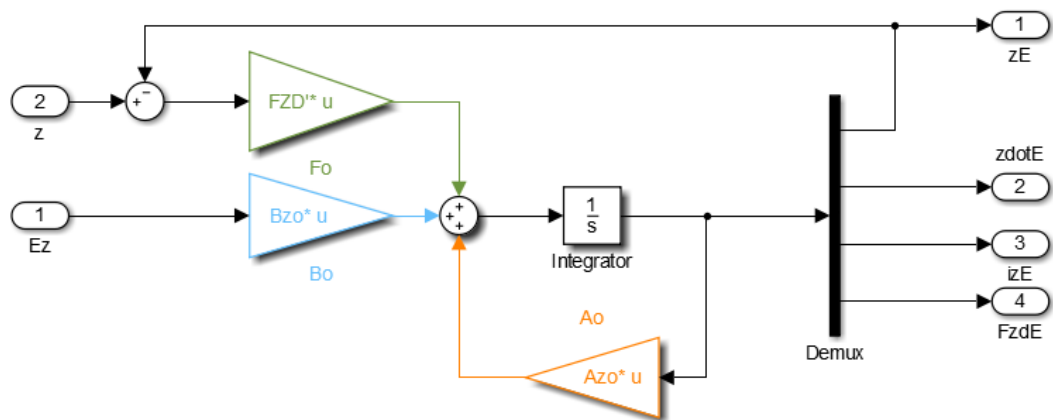
Figure 2.27 Disturbance Observer of z axis
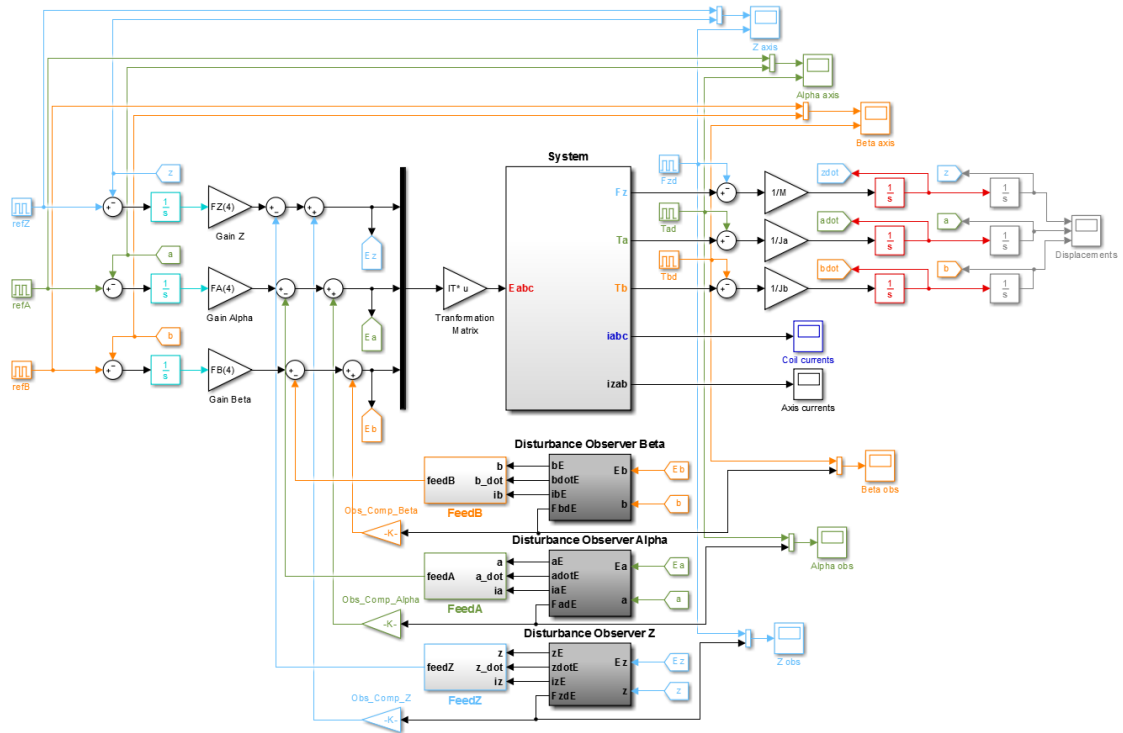
Figure 2.28 SSI control diagram with D.O. with compensation

Given the simulation results below, same setup is used to compare simulations for both systems. With disturbance compensation, system performs better when a disturbance is applied. Also faster response minimizes the current required. It can be assumed that with D.O. and compensation input, system is more stable, faster and efficient.
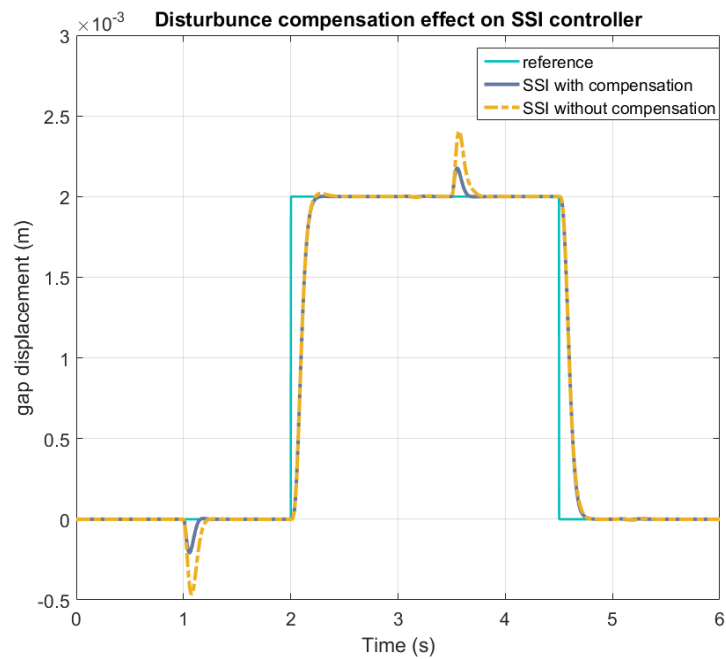
Figure 2.29 SSI controller response with and without disturbance compensation
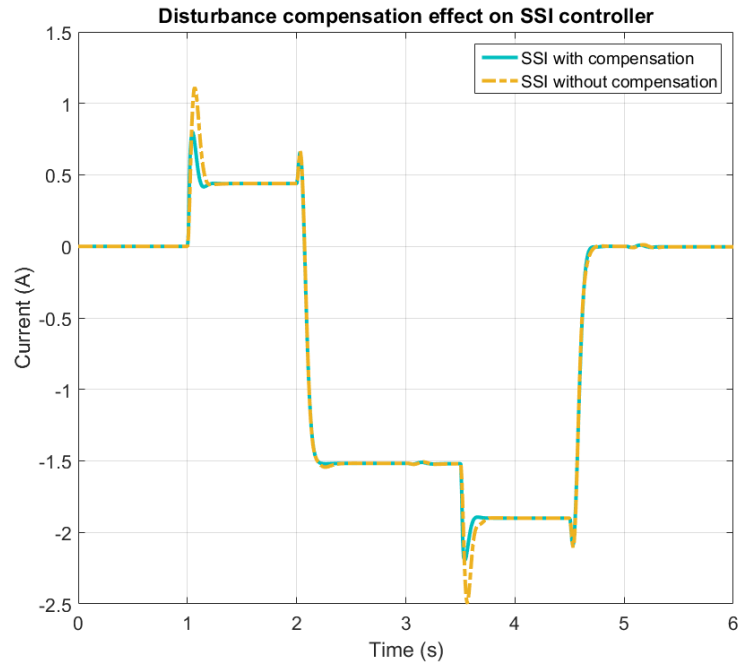
Figure 2.30 SSI controller currents with and without disturbance compensation

Zero power controller performs better with disturbance compensation like SSI. D.O. decreases reaction time and system responses faster. Faster zero power control algorithm settles faster, which also decreases required maximum current at peak points.
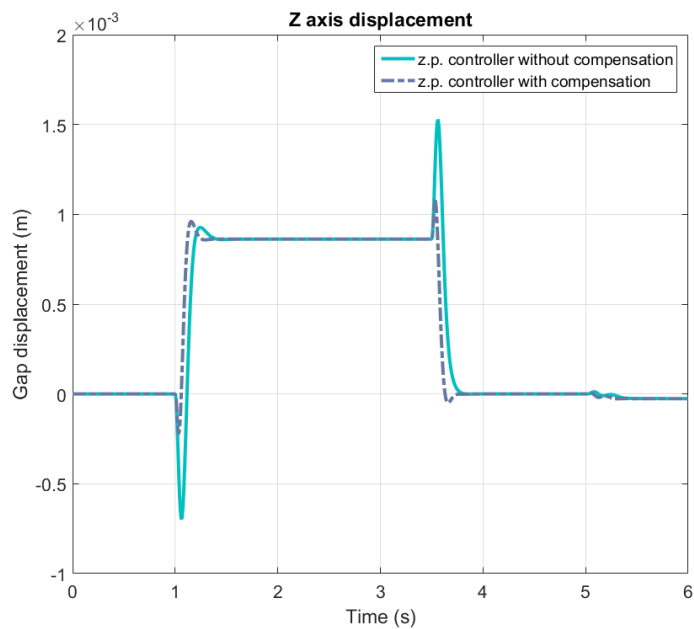
Figure 2.31 Zero power controller axis displacement with and without disturbance compensation
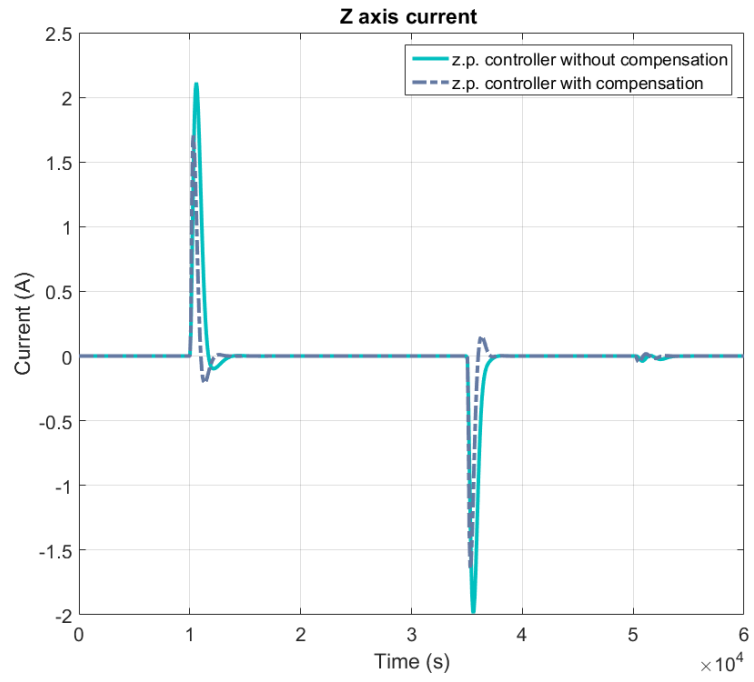
Figure 2.32 Zero power controller axis current changes with and without disturbance compensation

CHAPTER 3

FINITE ELEMENTS METHOD ANALYSIS AND SYSTEM DESIGN

Resulting from the fact that system has no friction surface, absorbing the disturbances with a mechanical suspension is not possible. As a result, all forces and moments should be applied uniform. Symmetrical design is the key detail. Moreover, symmetrical design makes modelling and controller much easier. Decentralized control algorithms can be applied in the same way to all poles and alpha and beta axes of centralized control algorithms will be similar. Because of this reasons, maximizing the efficiency of both system and background working, symmetric design is applied.

3.1 Physical Design and Improvements

The older system design template to work on has the same build consisting of three electromagnets and three linear motors. However positions of electromagnets lowers the moment arm length we model. The assumption is both head sides of u-type electromagnet applies same amplitude but opposite magnetic flux, which means developed forces are equal. As a result, resultant force can be modelled at the center of u profile. Older system's electromagnets point to the center of the mover, causing the length of moment arm to be less in length. To overcome this problem, electromagnets positions and the shape of placement are changed. Hybrid electromagnets aligned at the border of mover. Figure 3.1 shows the moment arm difference between first prototype and the reference study. Moment arm does not change because the distance to the center is equal in both the modelling of each pole force as separate and using resultant force. Figure 3.1 shows the new placement decided. Platform holds all system together, electromagnets and motors sizes are all equal.
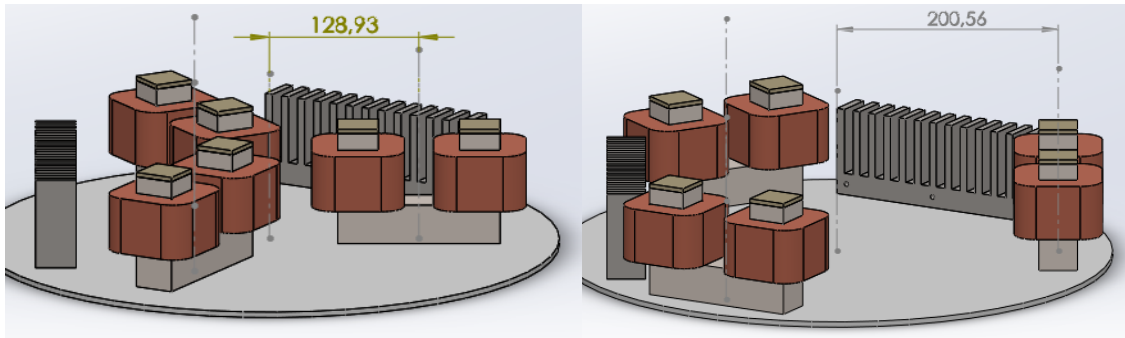
Figure 3.1 Moment arm difference over placement style (one linear motor on each study hide for better view, measured length is in mm)

After selecting the positions of placement, several types of U profiles are analyzed. Silicon steel's high density (around 7,8 kg/dm^3) makes system heavier. Heavier system need more force to move and higher gain controller and such (F=ma). Slimmer core means lower weight, but narrow cross section means flux saturation in terms. Several analyses are conducted to observe magnetic flux changing on cross section area. Trial analysis results showed magnetic flux saturation does not occur in working range. According to those results, thinner core can be selected.

However, proposed system used 35x35mm permanent magnets which is limitation. Thinner core and wider pole heads come up with as a solution. Proposed system design was in consideration on zero power control algorithm, so both experimental system and amplifier circuits for it. Considered maximum impulse to system should be from +5A to -5A so FEM analysis done in this limits. Thinner core has the capability of magnetic flux transmissivity. However, placing the permanent magnet on core with air gap around pole cause flux loss. As considered, wider pole head is our solution. Wider cross section near pole head leads the permanent magnets flux to flow cross pole head in core without loss. Only the cross section change zone can cause resistance, yet analysis show us this resistance does not affect a lot. Advantages of slimmer core are much more than disadvantages.

Each old electromagnet was 2,6 kg without coil according to FEM calculations. Second revision saved 1 kg on each electromagnet which performs in limits as well. Figure 3.2 show the Maxwell static electromagnetic analysis results. The analysis point is closer to railway than modelled point, yet flux scale is maximum yellowish. It can be admitted the new design achieve adequate results with lightweight. If it is taken cognizance of

collateral effects, slimmer core needs shorter and slimmer bolts, smaller nuts and shorter total length of core copper at same spin count, which make way of even lesser weight.
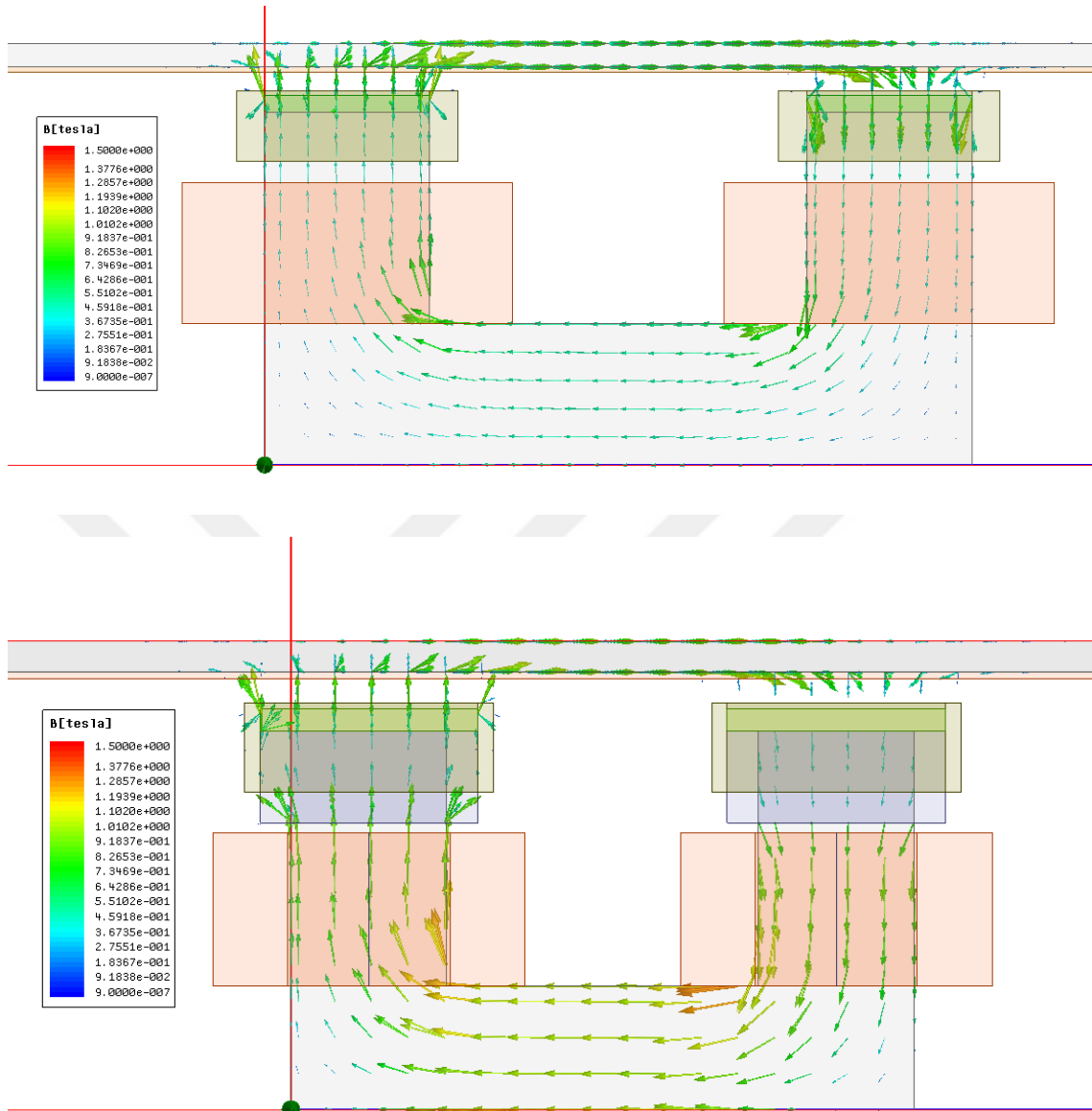
Figure 3.2 Reference (upper) and new (lower) prototype flux graphics.

In figure 3.2 the flux graphic fracture around head part had spotted. Magnetic flux happen to acted like fluid. Constriction and expansion cross sections cause deterioration. To investigate the expansion angle effect, parametric analysis performed. One of the analysis result is in figure 3.3 as an example. Leading flux at better angle to head and from head would give better performance, as thought. Force generated was equal at both types. As can be seen, magnetic flux graph is similar. Table of magnetic flux is missing for bigger image and more details.
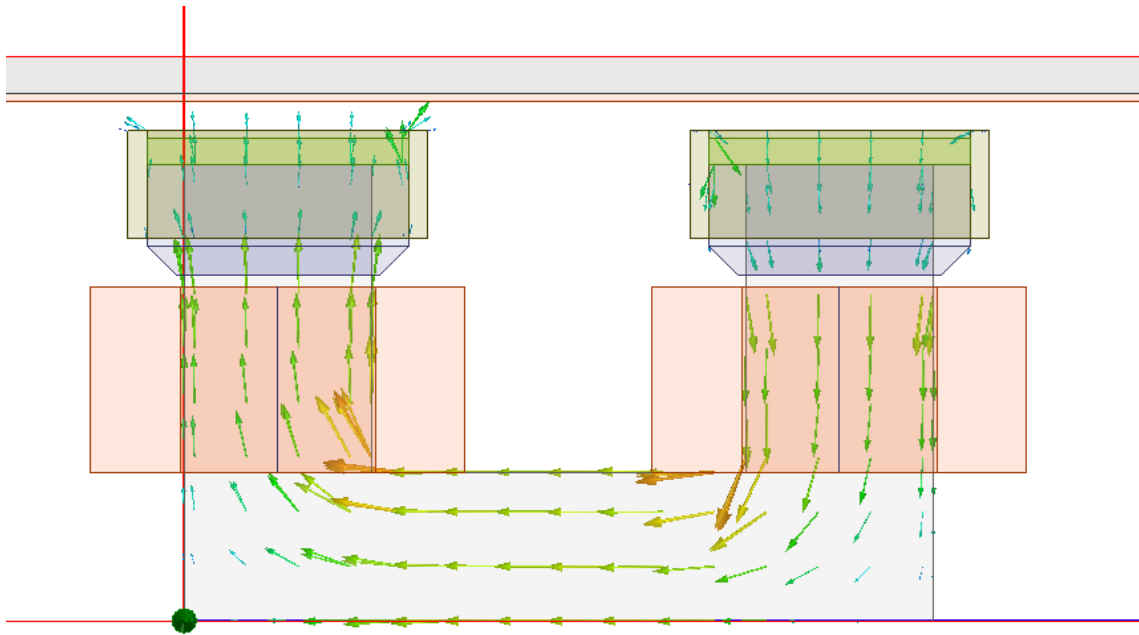
Figure 3.3 Angular expansion effects to magnetic flux current graphic

Angular change didn't effect as expected. Size of the head was high enough to compensate flux expansion. Corner losses did not affect force neither flux characteristics. According to this result, non-angular incremental build selected because of easier manufacturing, which end up the third revision of design.

The system has three hybrid electromagnets and three linear motors. All of them have silicon steel cores and coils, similar to each other. Manufacturing process and structures are nearly same, excluding coil numbers, electromagnets are one phase coils but linear motors three. Combining cores and lowering part number to develop a new structure which will be take part in literature.

Zero power control uses nearly zero input, very low total current. System works nearly passive. Because of this characteristic, it is considered placing the electromagnets on the linear motor would not affect motor driving.

Mainly new design had two builds. Placing the U type core at the middle of motor, and put motor coils exterior to electromagnets but this idea didn't advance. This kind of structure would cause high inertial moments along the core. Like the first revision, robustness and stability will decrease. For system efficiency and feasibility, pole heads placed to end points of linear motor core.

Last revision has motor coils inside and hybrid electromagnets at both ends. Simulations and FEM analysis showed, length between cross poles determine the force generated. Fewer the gap cause higher force. However if system is in limits, force loss can be accepted. Final design which manufactured and used in this study can be seen in figure 3.4.
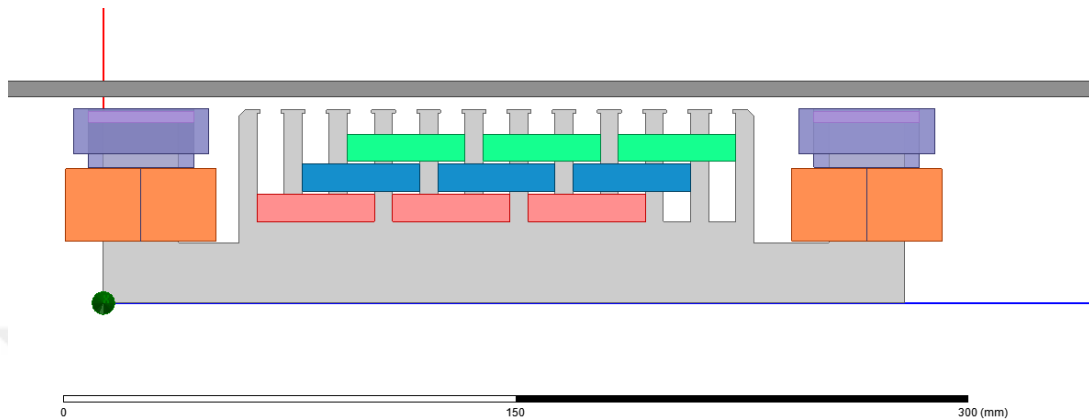
Figure 3.4 Hybrid combined linear motor electromagnet
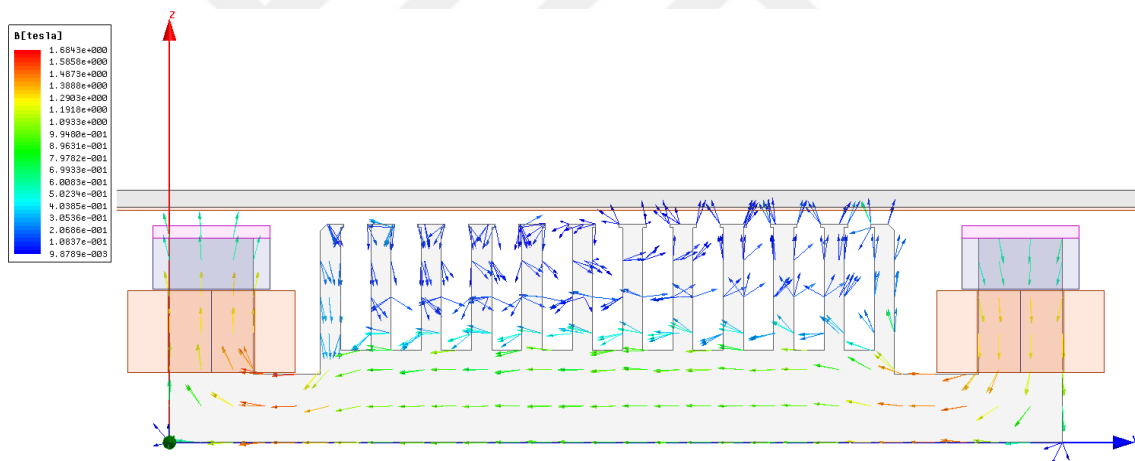
Figure 3.5 Magnetic flux loss at combine systems core

FEM analysis showed the force generated does not change much. As an example, second revision can hold the system levitated more than around half millimeters that is nearly same.

Last design had several advantages as such;

- Easier manufacturing,
- Cheaper manufacturing,
- Fewer parts for assembly.

3.2 Magneto static Levitation Force Analyses

Simulations helps to know system characteristics. Magneto static analysis calculates magnetic attraction force. Main purpose is making system to be hold in air only force gained by permanent magnets. To achieve this purpose, zero power point should be known. In this study, complete system is around 17kg (Solidworks mass calculations). 167N is required to hold system levitated. Table 3.1 shows the magneto static analysis results for single motor.

Table 3.1 (Force unit "N")

Ampere	2mm	3mm	4mm	5mm	6mm	7mm	8mm	9mm
5	328,22	258,73	208,03	169,81	140,53	117,51	99,07	84,26
4	312,71	244,00	194,42	157,28	129,00	106,91	89,66	75,87
3	294,38	227,20	178,97	143,32	116,56	96,04	80,09	67,43
2	273,50	208,14	162,09	128,60	103,94	85,14	70,65	59,20
1	249,77	187,56	144,63	113,96	91,55	74,57	61,49	51,28
0	224,31	166,69	127,51	99,71	79,50	64,41	52,84	43,90
-1	198,32	145,99	110,74	86,10	68,26	55,04	44,95	37,13
-2	173,06	126,32	95,23	73,61	58,05	46,53	37,84	31,10
-3	149,27	108,26	81,11	62,31	48,90	39,02	31,54	25,80
-4	127,61	92,00	68,58	52,48	41,00	32,57	26,24	21,38
-5	108,64	78,01	57,98	44,22	34,42	27,23	21,84	17,70

Table 3.1 (cont'd)

Ampere	10mm	11mm	12mm	13mm	14mm	15mm	16mm	17mm
5	72,29	62,48	54,36	47,57	41,90	37,09	32,99	29,45
4	64,80	55,78	48,32	42,11	36,97	32,58	28,89	25,72
3	57,36	49,15	42,40	36,81	32,19	28,29	24,99	22,16
2	50,10	42,74	36,72	31,76	27,65	24,23	21,33	18,84
1	43,20	36,69	31,40	27,04	23,47	20,46	17,96	15,82
0	36,78	31,12	26,52	22,74	19,66	17,07	14,91	13,09
-1	31,01	26,08	22,15	18,91	16,25	14,05	12,21	10,67
-2	25,83	21,64	18,26	15,52	13,27	11,41	9,87	8,57
-3	21,34	17,79	14,95	12,64	10,76	9,19	7,91	6,83
-4	17,59	14,59	12,19	10,27	8,69	7,39	6,32	5,43
-5	14,49	11,96	9,96	8,33	7,01	5,93	5,05	4,31

According to analysis results, system can be levitated from 4mm (-5 A limit) to 12mm (+5 A limit) (Total mass / 3 for symmetrical forces, equals 55 N). However, this study aims to achieve zero power control. Between 7mm and 8mm is the point of zero power levitation.

Results show us the nonlinear characteristics of maglev systems. At 2mm, total force change is around 200N within 10A range, but at 17mm gap force change is 25N.

CHAPTER 4

MANUFACTURING PROCESS

According to analysis results, the final build has sufficient performance needed. Magnetic flux graphics show us, smaller dimensions are still in workable limits. Because of easier production and less parts, the final mixed core has been selected for experimental build.

Complete experimental mechanism requires mover which contains the hybrid electromagnets with motors and displacement sensors with calibration PCB, iron rail core with copper coating and base platform to carry the whole system. Figure 4.1 shows the experimental design of mover, drawn with CAD design program SolidWorks. Computers and controller boards are placed close to each other for unexpected situations.
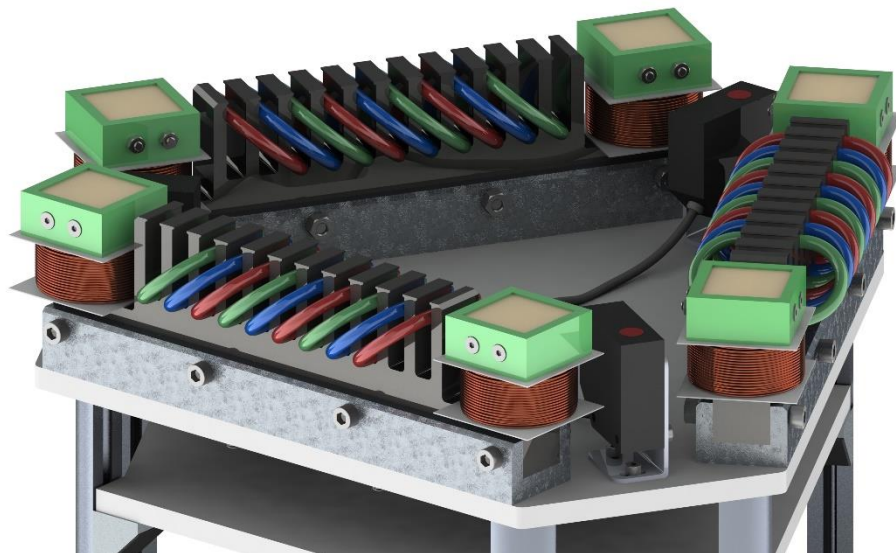
Figure 4.1 CAD design of experimental build

4.1 Mover

Although magnetic levitation systems contain fewer parts, each part requires precision fabricating. Proposed system was calculated to levitate at around 5mm air gap. 0,5mm of disturbed surface equals 10% of working limit, which is endangering system linearity.

The first step of manufacturing is core assembly. Electric steel, which is called "silicon steel" is one of the most used materials for cores. Core comprises of several laminated silicon steel to overcome hysteresis loss.

Magnetic properties of electromagnet causes heat loss called hysteresis loss. When an armature core is in a magnetic field, magnetic particles inside the core line up with the magnetic field. When the magnetic field rotates, continuous movement of the magnetic particles produces molecular friction. This produces heat and this heat is transmitted to the windings. The heat changes the armature resistances and increases with temperature.

Relation between power loss and hysteresis loop area.
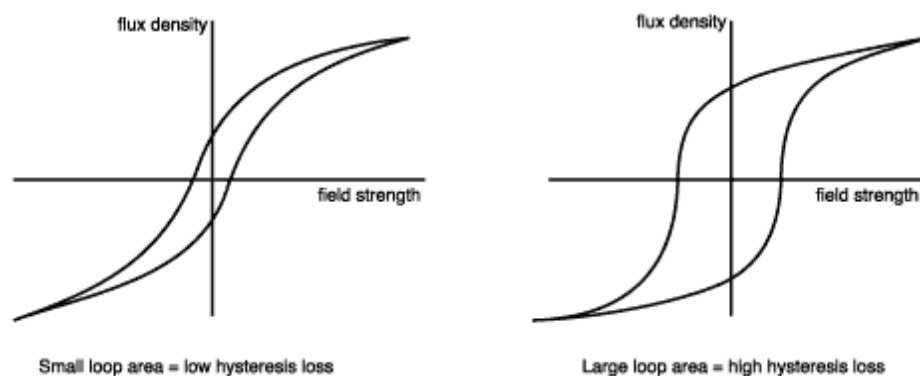
Figure 4.2 Hysteresis loss, difference between small loop areas to large loop area

Because of easier fabrication and availability, 0,5mm thick silicon steel has been chosen. By an easy calculation, each mixed motor core requires 50 lamination to complete 25mm thickness of designed form. However, unexpected burr or figure disorders can occur. With regard to fabrication tolerance, each part number is multiplied by 1,2 safety factor. 180 lamination for each motor fabricated for this project.

Manufacturing methods searched of optimal solution; precession, price and availability. EDM (electrical discharge machining) cutting is expensive and not efficient on thin parts. Water jet cutting is not suitable for cutting laminations of steel because of oxidation. Mold cutting is expensive for fewer parts. Laser cutting has enough precision for proposed manufacturing process (0.1mm according to workshop ordered), so laser cutting is

selected for fabrication of motor cores. Figure 4.3 shows the laminations and completed package of motors.

Figure 4.3 Silicon steel lamination and package of motor

Because of burr from cutting, one package (consist of 50 lamination) was about 28mm, which is 3mm thicker than calculation. Each lamination surface was grinded using sandpaper by hand. After the process, package thickness is lowered to approximately 25mm. All packages completed, compressed and send to coiling. Before the coiling process, each motor painted for corrosion and oxidation.

Figure 4.4 Painted core with motor coils

However, the painting coat wasn't implemented by spray coating or static coating but brush which cause increase of thickness and non-uniform surface. This unwanted problem was solved by removing one lamination from each cores. In order not to damage coils, lamination removal was done by cutting the edges and ripping off several parts.

After the coiling and resin coating, cores are seated in aluminum bases. Those bases are crafted from single aluminum block by milling. To protect the permanent magnets from damages, 3D printed blocks are placed at the top of motor to face the vibrations and impacts at experimental optimizations. An example of one completed core with bases, protectors and coil groups is given in Figure 3.5. Motor has 9 coils, 3 sets for each phases. Each phase coils are connected in serial. Each motor phase has 8 ohm resistance and each electromagnet has 2 ohm resistance by cross serial connection. To create opposite poles on hybrid electromagnets, current should be clockwise on one magnet and anticlockwise on other, so that coil serial connection is different from motor phase connections.
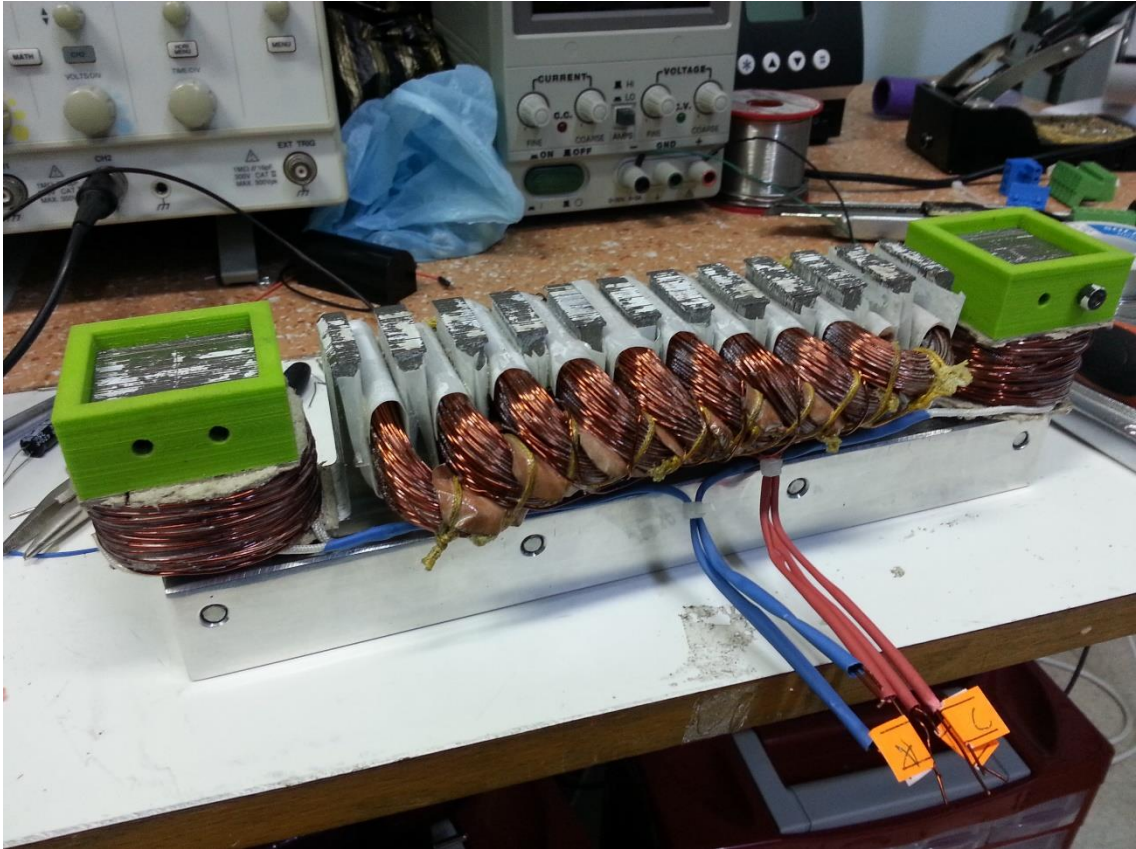
Figure 4.5 Completed mixed core without permanent magnets

Last part of mover is the main base, which is laser cut from 5mm thick aluminum plate. Static force analysis show us (Solidworks Simulation) 5mm thickness is durable enough for our system. Burr and defected surface are cleaned with sandpaper; motors and OMRON Z4W-V displacement sensors' bases are placed on main base. For future experiments, PCBs and other electrical components (including motor drivers, embedded controllers and power sources) will be placed on the mover. Also different types of sensors and controller can be load on mover. So that design should changeable whenever needed. For first steps, sigma kind 20mm aluminum profile used for column of cabinet and plexiglas layers are fixed. Enclosing layers and decorative improvements can be done after succeed of study. Figure 4.6 shows the final mover.

Figure 4.6 Completed mover (without sensors)

4.2 Base and Passive Track

Magnetic levitation requires ferromagnetic track to induct magnetic force. 5mm and thicker iron track is enough for levitation according the analysis results. To reduce the cost and mobility and also for safety reasons, 8mm track is selected. Table 4.1 shows force differences over thickness of induction plate. FEM calculations are done at 4mm air gap, 3A pole currents each. Force is given in Newton. (For faster calculations, mesh parameters are set automatic which cause error at 9mm, but it is enough to confirm the idea.)

Table 4.1 (Force unit "N")

2mm	3mm	4mm	5mm	6mm	7mm	8mm	9mm	10mm
112,51	124,55	126,94	127,88	129,09	129,18	130,48	130,01	130,63

Because the proposed system has 6 DOF, it can move on both axis on track so, conveyance track should not be limited with the movement mechanically. To avert this problem, 2 types of tracks are designed. One dimensional movement requires at least the size of mover, which we called linear track. For planar movement, track should be wider

than linear track. We chose 2 times width of linear track, which gives us easier fabrication. We designed 5-piece iron layers sized 800mm*450mm, which form a rail system with one planar and three linear tracks. Each track of iron is around 20,5kg and cut with laser for precision at hole orientation. Hand drill may cause a displacement between them. Each plate is mounted with countersink bolts for a smooth surface. Regular bolts cannot be used because;

- If bolt is higher than air gap, mechanical crash will occur,

- If bolt is not higher than air gap, sensors will fail at bolt head and

- Force will peak at bolt heads and will cause levitation failure.

Similar to mover, some drawers are needed in experiments. Mover should be high enough from ground for easier experiments. Sigma aluminum profiles (45*45 and 45*90) are used to construct the track system as 1300mm high from ground. Figure 4.7 shows the track system.
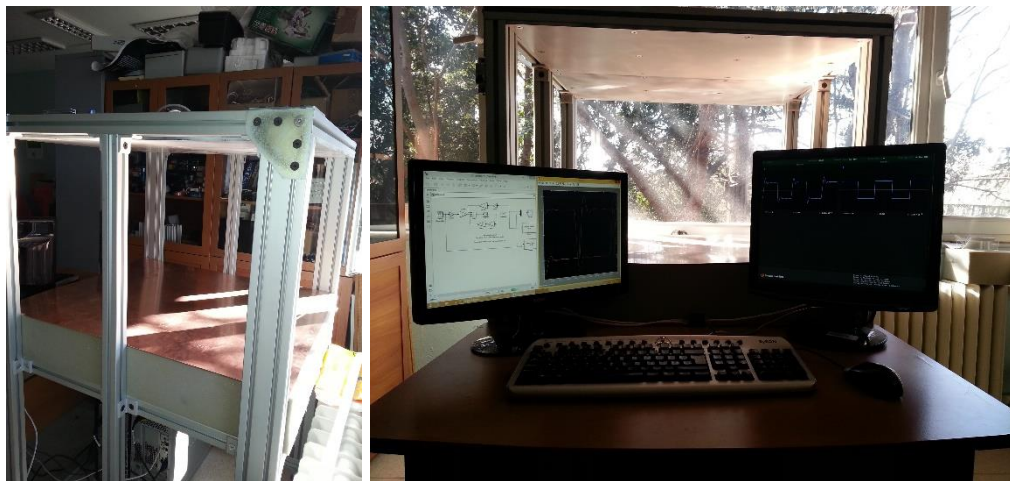

Figure 4.7 Aluminum profiles and rail (left), complete experimental system (right)

4.3   Electrical Components

To achieve the complete control of the system, these electrical components are required;

- Levitation (hybrid electromagnet) controller
- Trust (motor) controller
- Power source and computers

4.3.1 Levitation Controller

Levitation controller can be divided into two parts: power electronics and controller algorithm with controller board. OPA549-T based linear amplifiers are used to drive electromagnet coils. Power electronic circuit accepts analog input, which also determines the controller board type. Op-amp driver uses inverter output, which cause positive input to negative output, but this is recalibrated by the software. Also further experiments might be done with embedded controllers. To achieve this goal, gain of driver is calculated. Regular microcontrollers outputs 5V and newer models 3.3V. 5V are selected and limited the controller to output 5A. Each coil is 2,6 ohm. Easiest calculation is with Ohm's law; (V0 is required voltage, Vm is microcontroller output and G is gain. Unit of V0, Vm is volt, R is ohm and I is ampere)

$$V0 = I * R$$

$$V0 = 5 * 2,6$$

$$V0 = 13 \ V$$

$$V0 < Vm * G$$

$$13 < 5 * G$$

$$G > 2,6$$

Selecting the resistors of op-amp drivers should be 2,6 times higher. Selecting 3 times gain, which gives maximum 5,7A output with 15V feed input.

Figure 4.8 OPA549-T amplifier linear driver and sensor interface board

As seen from figure 4.8, Op-amp driver has in-build modes and current limiters. This driver can be used as voltage type and current type. Both applications can be used with required software readjustment. Each op-amp driver is limited to 10A by hardware for security reasons. Also software saturation filters are added as a secondary security layer.

Three coils (crossed serial connected for each motor) requires three op-amp to be driven. Each op-amp can be driven with analog output from controller board, at least three analog output is required for levitation.

Control algorithm uses sensor information as feedbacks from system effects and reactions. System has three displacement sensors and for further observations three current sensors are used, which indicates us at least six analog inputs are required.

NI PCI-6259 and NI PCI-6733 configuration has the required outputs and inputs. Also this controller boards are fully supported by MATLAB Simulink real-time control algorithm method. For accurate control and easier calibrations and changes applying to system, Simulink and NI controller cards conjunction is ideally suited. Connector board are shown in Figure 4.9, DAQ cards are slotted inside controller PCs PCI slots.

Figure 4.9 NI DAQ controller connector board (1 for PCI-6733, 2 for PCI 6259)

4.3.2 Trust Controller

Trust controller has the same build like levitation controller; power electronics and controller electronics.

Hence the motor driver outputs sinusoidal wave form, which means continuously changing direction of current, H-Bridge motor driver can be used efficiently.

The term H-Bridge has its name from the structure of itself. Four MOSFETS or transistors are placed at two upper and two lower parts and motor is placed perpendicular between lower and upper layers which gives exactly the form of "H" letter. Switching the gates crosswise, current flow changes direction, which changes the DC motor's direction of rotation. Figure 4.10 is an example to circuit diagram of logic behind the H-Bridge.
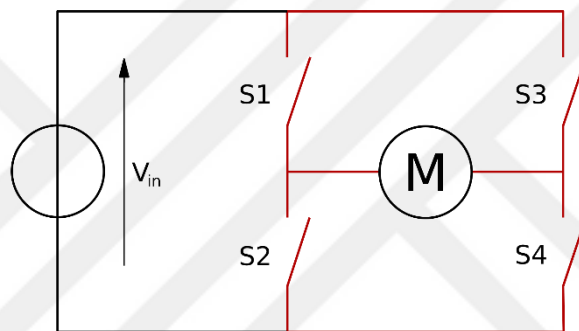

Figure 4.10 H-Bridge circuit diagram (crosswise directions are S1-S4 and S2-S3)

Proposed system has three three-phase-motor, which means three three-phase drivers or nine one-phase drivers are required.

This system build is completely new and "patent pending". Each affect should be discretely observed and controlled separately. Nine one-phase drivers will give the freedom looked for. Each wire and driver can be observed separately Also for further experiments and different test platforms those designed motor drivers can be used. H-Bridge drivers are built for higher capacity.

100V 10A output, which is roughly 1kW, higher resistance motors can be driven. But higher capacity makes card bigger; bigger MOSFETS and other electronic components. Also high power cause heat load. High temperature can damage semiconductors and burn drivers itself. Active cooling is required. Figure 4.11 shows the H-Bridge card, which had three layers; one controller, driver and power supply.

Figure 4.11 One phase 1kW motor driver

Nine 1kW driver needs its own shelf. Several shelves are connected to support aluminum bars forms the frame of drivers. Cable management and assembly of drivers can be seen from figure 4.12 to 4.14.

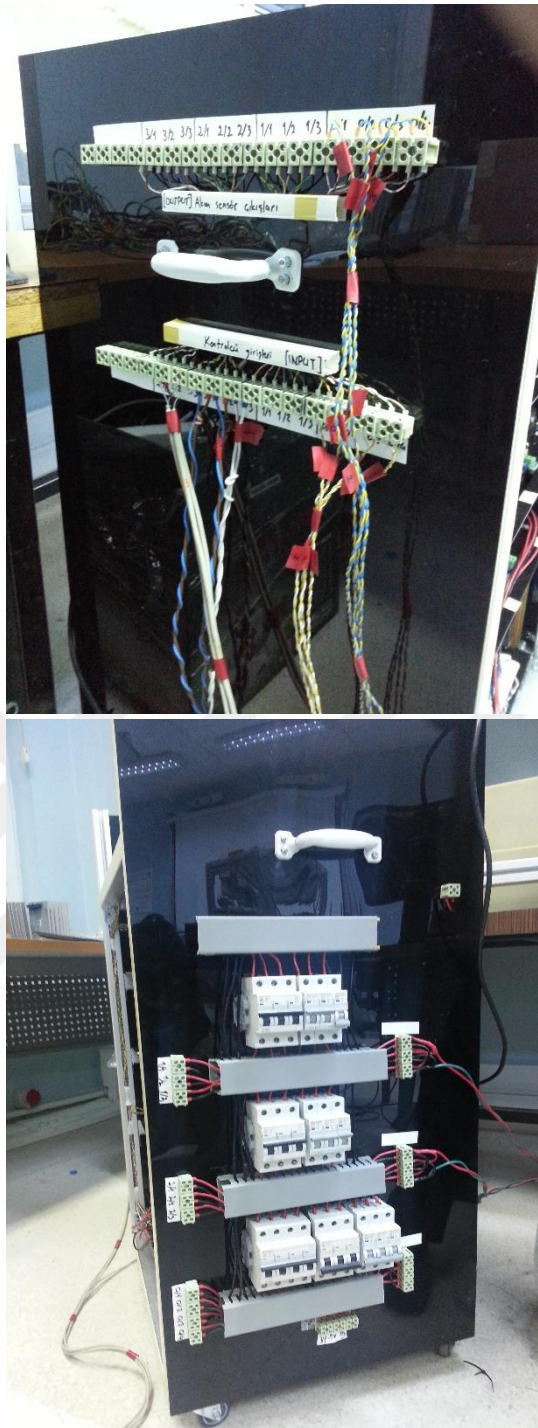Figure 4.12 Motor drivers cable management and cooling fans (3 shelf)

Figure 4.13 Outputs, inputs for Quanser and fuse system, high voltage inputs

Figure 4.14 Complete system, three shelf H-Bridge driver and one shelf linear driver

4.3.3 Power Source and Computer

As calculated before, at maximum trust driving system can drain up to 3A continuous and peak 5A on each phase. To achieve 5A, voltage driven system requires at least 24V voltage source. Mixed current drain can be up to 45A for all motors' all phases run at maximum current. Power source for trust controller can be chosen as 24V 50A.

For levitation, each electromagnet can drain up to 3A continuously and peak 6A for short time periods. There is total three electromagnets, 18A is required on the edges of system. Power source for levitation system can be chosen as 15V 20A.

Figure 4.15 Trust controller power source (right) and levitation controller power source (left)

MATLAB Real time controlling can be applied with xPC target build. Advantages of xPC are;

- High sampling frequency
- Robust standalone controller hardware
- Lower performance CPU's can be used

However, using two PCs is a must. Operating two computers does lower the efficiency. Further experiments will be applied on embedded systems, which will lower the PC number to one and to none. According to literature study, embedded controllers can be used with smart phones or tablets over Wi-Fi, Bluetooth etc. Also autonomous algorithms can be applied and system can run itself, only sending data over communication protocols.

CHAPTER 5

EXPERIMENTAL RESULTS

The goal of this thesis is to apply centralized zero power control to system. However experimental studies better applied from easier to complex. First levitation with easy control methods are applied and complex control methods follows.

5.1   Levitation

In chapter 4, experimental setup is explained. Total experimental setup has two PCs, one for real-time controlling with DAQ cards slotted and one for tracking the controller and making required changes.

xPC target computer does not have an operation system installed. Required communication settings and user interface boots from CD or USB stick.

Main computer has controller algorithms written in and has the capability of running controller applications. In this study, MATLAB with Simulink is selected for controller applications. This application compiles the controller program to a language target computer can understand and sends via Ethernet.

xPC can run standalone or connected to the main computer. Experimental setups usually does not disconnect, because different controller parameters can be applied and results observed.

Omron Z4F-W used for gap measurement; however, a transform equation should be written. Output of sensor varies from 4mA to 20mA according to -4mm to +4mm. DAQ input accepts voltage as signal. Gap calibration PCB has 250Ω at output, which settles 4mA to 1V and 20mA to 5V.

Even with precise mechanical position calibration, there can still be unbalance. Figure 5.1 shows the complete sensor block diagram. Gap adjustment should be separately calibrated since it is required.
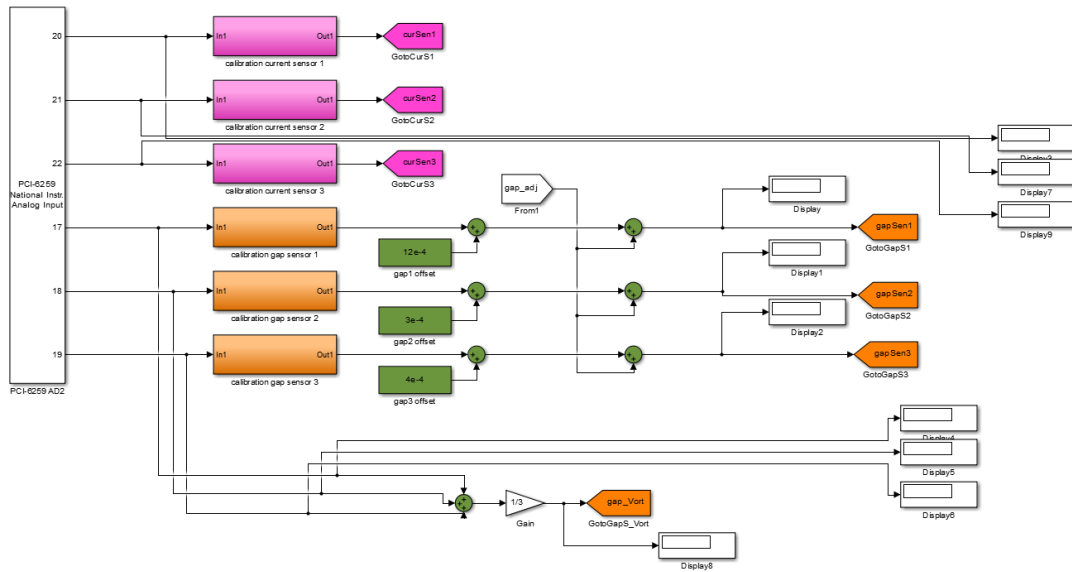

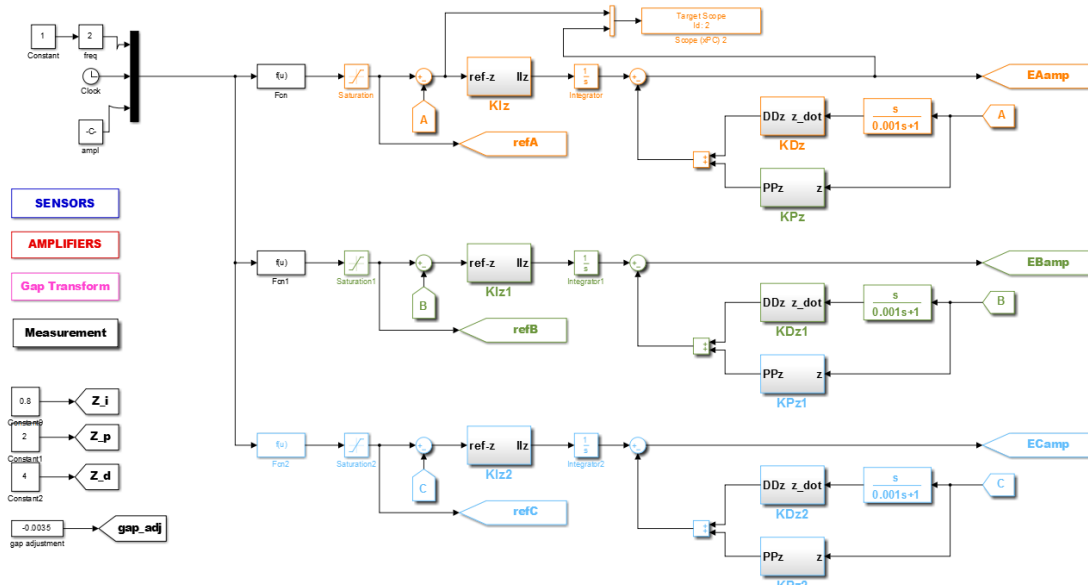Figure 5.1 Sensor calibration blocks

5.1.1 I-PD

Figure 5.2 Experimental decentralized controller block diagram

Similar to simulations, both decentralized and centralized control can be applied to experimental study. Decentralized control can be applied more easily because of

individual force algorithm. First setup is decentralized control with required calibration transforms.

Table 5.1 Calibration test

Input	DAQ output	Measured voltage	Measured current	DAQ input	Sensor output
3	3,030	-8,220	-3,685	3,680	3,650
2,5	2,530	-6,920	-3,110	3,510	3,474
2	2,020	-5,540	-2,527	3,330	3,295
1,5	1,520	-4,150	-1,918	3,150	3,102
1	1,010	-2,760	-1,285	2,950	2,907
0,5	0,488	-1,370	-0,644	2,740	2,705
0	0,010	0,150	0,000	2,540	2,503
-0,5	-0,510	1,430	0,641	2,350	2,305
-1	-1,010	2,820	1,280	2,150	2,102
-1,5	-1,510	4,200	1,911	1,950	1,908
-2	-1,990	5,580	2,525	1,750	1,720
-2,5	-2,480	6,930	3,095	1,580	1,542
-3	-2,990	8,350	3,610	1,410	1,372

OP-Amp circuit has high power inverting setup with around 2,7 gain. Current sensor outputs from 0V to 5V but linearity can be changed within range. First order or second order polynomial fit can be applied for calibration. MATLAB has build-in function called "polyfit" for this calculation. Each sensor characteristic are determined before and after fit operation and first order (y=ax+b) polynomial fit had enough precise and selected for less calculation load to PC.

After input and output calibrations are complete, one of the most important experiment is to estimation of k parameter done. For this estimation, several layers of Plexiglas are put between electromagnet and rail and obtain the current value where system drops. This

experiment is done with ramp function, where current starts from positive value to negative.

Table 5.2 Linearization test

Gap	5,7	6,9	8,1	9,3	10,5	11,7
Current	-4	-2,3	-0,2	0,7	2,2	3,7

After linearization test is done, k parameters are found and with this value K_x and K_{ix} parameters are calculated. These parameters are put in their equations and controller is calculated. Test shows us around system zero power point is close to 8,5mm. However real gap is measured from core to rail. Real gap is 8,5+permanent magnet height+other layers, in this study permanent magnet is 3,5mm thick and securing layer is 1mm thick. Real zero power gap is around 13mm.
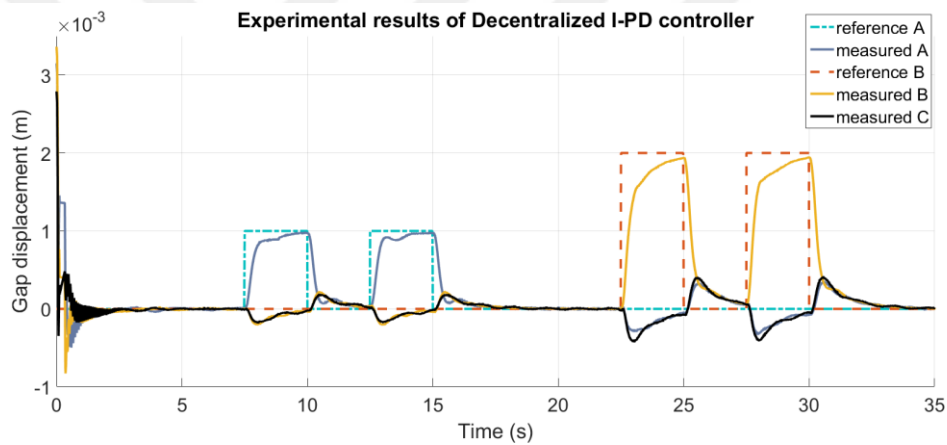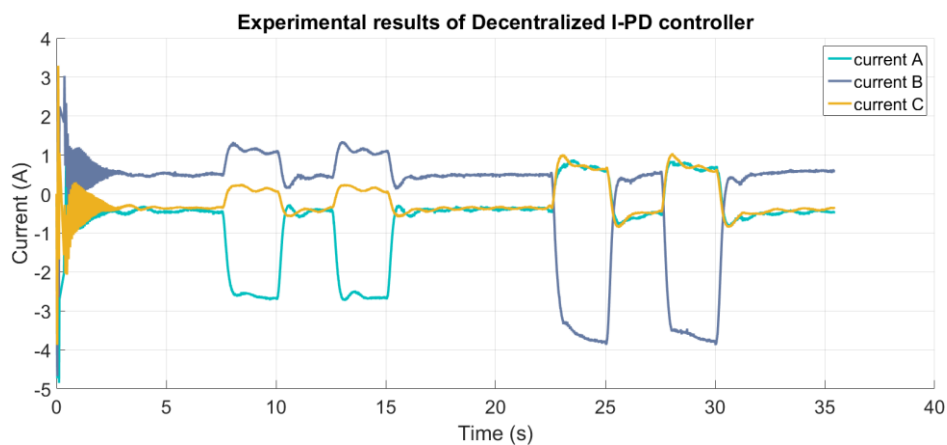

Figure 5.3 Gap displacements of experiments

Figure 5.4 Current changes of experiments

57

Figure 5.2 and 5.3 shows the first experimental results. At start, system drops itself from 3mm to 0 point. After steady state is confirmed, at 7. second reference 1mm step is applied to magnet A. At 16. second reference is cancelled, and at 23. Second 2mm step is applied to magnet B.

Figure 5.5 Levitating system

In secondary experiment, 120 degree phase shifted three sinusoidal references are applied to each magnet separately.
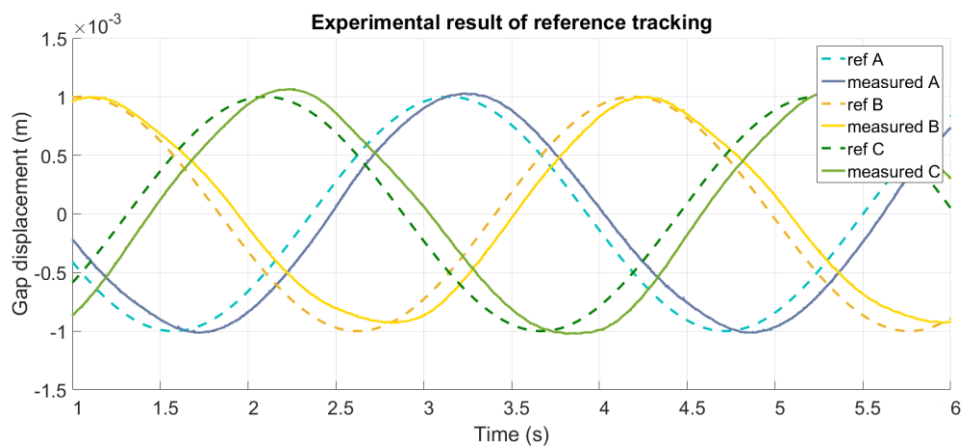

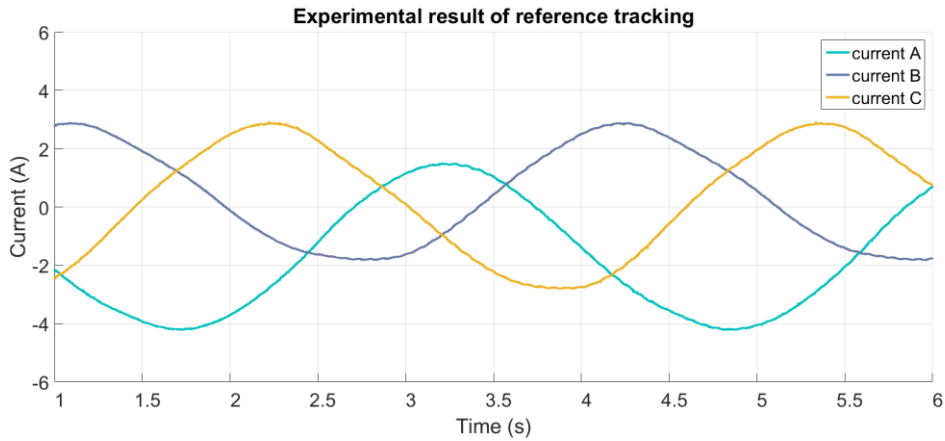Figure 5.6 Sinusoidal reference tracking of experiment 2

Figure 5.7 Sinusoidal reference tracking of experiment 2

As seen from figure 5.6 and 5.7, experimental reference tracking is confirmed, around 0,2 seconds shifted. Currents are not calibrated as it should be done, which cause unbalanced steady state currents.

First experiments shows system does levitate but this approach limits the performance. Control algorithm can be improved with centralized control which includes axis transformations. Centralized I-PD controller experimental results are given in figure 5.8, 5.9, 5.10 and 5.11.
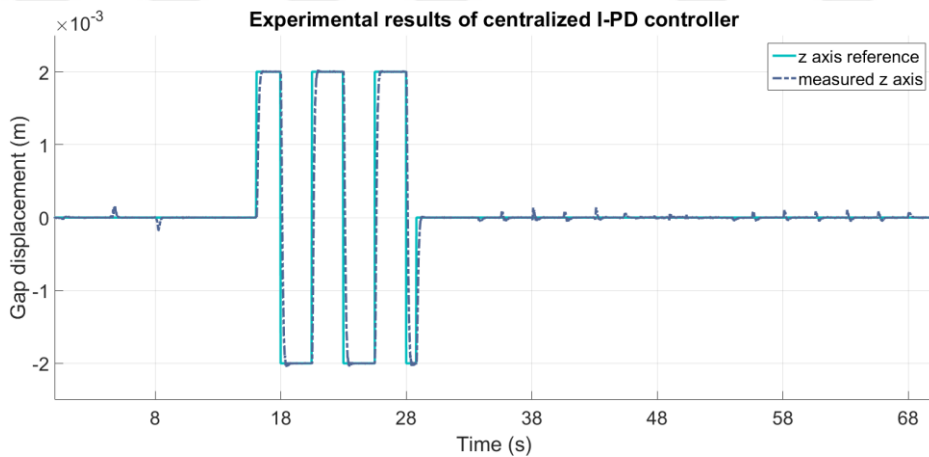

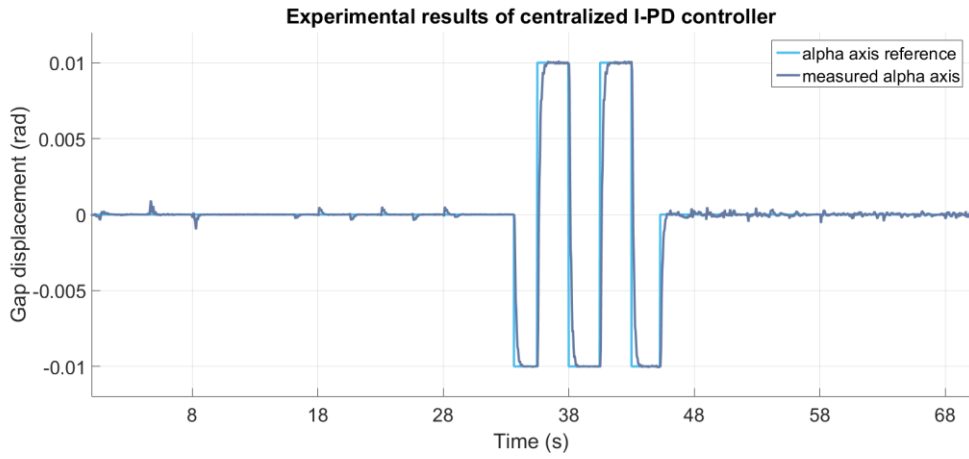Figure 5.9 Z axis reference response of centralized I-PD controller

Figure 5.10 Alpha axis reference response of centralized I-PD controller
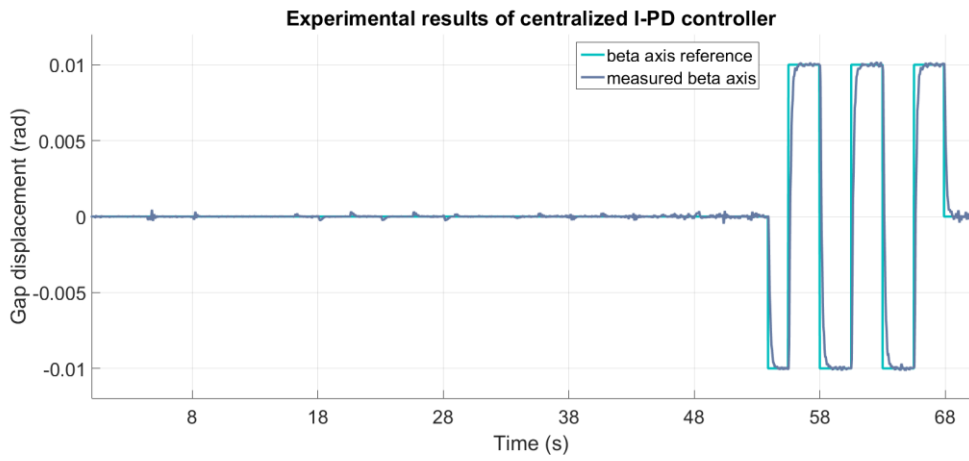

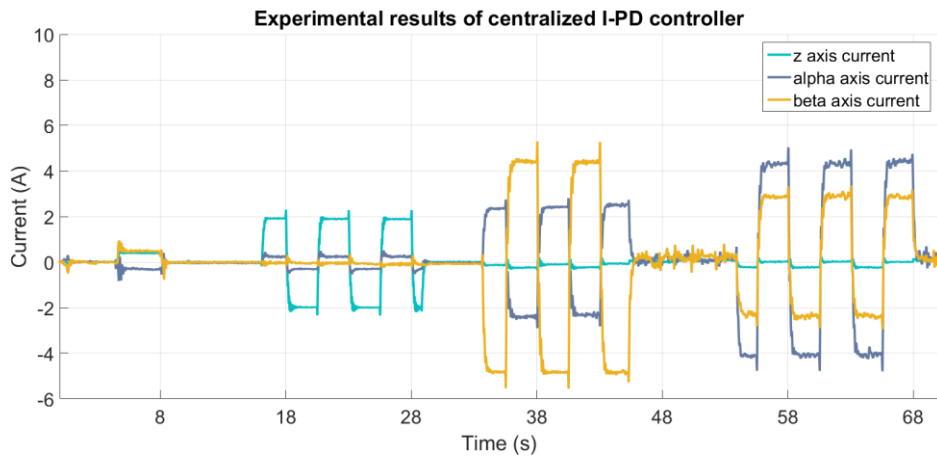Figure 5.9 Beta axis reference response of centralized I-PD controller

Figure 5.11 Centralized control axis currents

As seen from the results, centralized control makes system more robust than decentralized control. Inertia affects and axis couplings are included and controlled. Experimental build has several steps;

- 0.3 kg disturbance is applied at 5th second, removed at 8th second,

- 2 mm z axis reference is applied at 16th second, removed at 29th second,

- 0.01 rad alpha axis reference is applied at 32nd second, removed at 45th second,

- 0.01 rad beta axis reference is applied at 44th second, removed at 68h second.

5.1.2 Zero Power Control

Zero power control is a different method of SSI control algorithm. Controller parameters calculates similar. Experimental build has D.O. for more robust build and the compensation input to increases the stiffness of system. Experimental results are given in figure 5.12 and 5.13. After the steady state occur, 1 kg mass is placed in the middle of mover and removed after steady state reached. Same mass is placed the furthest alpha axis point and removed as well. Lastly the mass is placed furthest beta axis point and all results observed.
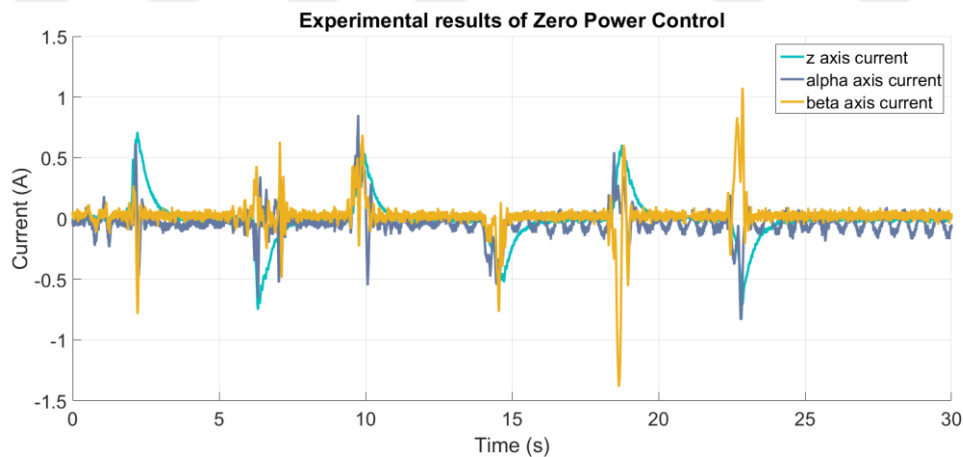
Figure 5.12 Zero power controller current responses
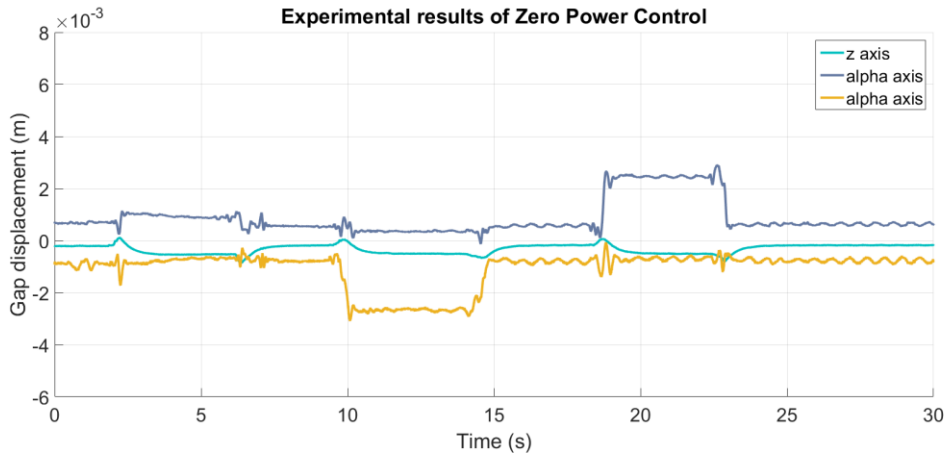
Figure 5.13 Zero power controller gap responses

Figure 5.12 shows us the currents remain at 0 at steady states. At loading times (2nd second for z, 9th for alpha and 18th for beta), system drawn current and changes the gap to overcome current error.

These results verify the implementation of both I-PD and zero power controllers are correct. However especially axis currents of alpha and beta seems coupled, which is unexpected. Sensor positions and transformations can be changed and different transformation method may performance better. Moreover coupling effect can be modelled for a new plant implementation.

REFERENCES

[1]   Sinha, P. K., (1987). Electromagnetic Suspension, Dynamics and Control, Peter Peregrinus, Ltd., London, U. K.

[2]   Boldea I. and Nasar S. A., (1997). Linear electric actuators and generators, Cambridge University Press

[3]   Morishita M, Azukizawa T, Kanda S, Tamura N and Yokoyama T, (1989). A new Maglev System for Magnetically Levitated Carrier System, IEEE Trans. Vehicular Technology, 38(4): 230-236

[4]   Ertuğrul, H. F. (2014). 4 Kutuplu 3 Serbestlik Dereceli Karma Elektromıknatısın Modellenmesi ve Kontrolü, MSc. Thesis, İstanbul Technical University, Graduate School of Natural and Applied Sciences, İstanbul.

[5]   Choi, J. S. and Baek, Y. S. (2008). Magnetically-Levitated Steel-Plate Conveyance System Using Electromagnets and a Linear Induction Motor, IEEE Transactions on Magnetics, 44(11): 4171-4174.H. F. Applied Sciences, İstanbul.

[6]   Kim, C., Lee, J., Han, H. and Kim, B. (2011). Levitation and Thrust Control of a Maglev LCD Glass Conveyor, IECON 2011 - 37th Annual Conference on IEEE Industrial Electronics Society, 610-615.

[7]   Hayashiya H., Ohsaki, H. and Masada E., (1999). A Combined Lift and Propulsion System of a Steel Plate by Transverse Flux Linear Induction Motors, IEEE Transactions on Magnetics, 35(5): 4019-4021.

[8]   Lin F. J., Teng L. T. and Shieh P. H. (2007). "Intelligent Sliding-Mode Control Using RBFN for Magnetic Levitation System", IEEE Transactions on Industrial Electronics, 54(3): 1752-1762.

[9]   Lin F. J., Chen S. Y. and Shyu K. K., (2009). "Robust Dynamic Sliding-Mode Control Using Adaptive RENN for Magnetic Levitation System", IEEE Transactions on Neural Networks, 20(6): 938-951.

[10]   Sun Z. G., Cheung N. C., Zhao S. W., ve Gan W. C., (2009). "The Application of Disturbance Observer-based Sliding Mode Control for Magnetic Levitation Systems", J. Mechanical Engineering Science, 224(8): 1635-1644.

[11]   Mizumoto I. and Tanaka H., (2010). "Model Free Design of PFC for Adaptive Output Feedback Control and Application to a Control of Magnetic Levitation System", IEEE International Conference on Control Applications, 35-40.

[12] Wai R. J. and Lee J. D., (2009). "Robust Levitation Control for Linear Maglev Rail System Using Fuzzy Neural Network", IEEE Transactions on Control Systems Technology, 17(1): 4-14.

[13] Erkan K. and Koseki T., (2007). "Fuzzy Model-based Nonlinear Maglev Control for Active Vibration Control Systems", International Journal of Applied Electromagnetics and Mechanics, 2007(25): 543-548.

[14] Erkan K. and Koseki T., (2005). "Flexible Nonlinear Stabilizing Control for Magnetic Levitation Based on A Fuzzy Algorithm for Safe and Comfortable Suspension of A Stage", COE Symposium, 2005, Tokyo, 383-387.

[15] Erkan K. and Koseki T., (2005). "3 Degrees of Freedom Fuzzy Model-Based Nonlinear Control of Triple Configuration of U-Type Hybrid Electromagnets", The 5th International Symposium on Linear Drives for Industrial Applications, 338-342.

[16] Ertuğrul, H. F., Okur, B., Erkan, K., and Üvet, H. (2013). "An Evaluation of Zero Power Controlled Maglev Systems for Flexible Conveyance", International Advanced Technologies Symposium (IATS), İstanbul-Türkiye, 457-461.

[17] Hajjaji A. E. and Ouladsine M. (2001). "Modeling and Nonlinear Control of Magnetic Levitation Systems", IEEE Transactions on Industrial Electronics, 48(4): 831-838.

[18] Baranowski J. and Piatek P., (2008). "Nonlinear Dynamical Feedback for Motion Control of Magnetic Levitation System", Power Electronics and Motion Control Conference, EPE-PEMC 2008. 13th. IEEE, 1446-1453.

[19] Ishtiaq, A. and Javaid M. A. (2010). "Nonlinear Model and Controller Design for Magnetic Levitation System", Proceedings of the 9th WSEAS International Conference on Signal Processing, Robotics and Automation, 324-328.

[20] Baranowski J. and Piatek P., (2011). "Observer-based Feedback for the Magnetic Levitation System", Transactions of the Institute of Measurement and Control, 34(4): 422-435.

[21] Liu, C. T., Lin, S. Y. and Yang, Y. Y. (2008). On the Fuzzy-based Control strategy Design and Implementation of a Non-contacting Steel Plate Conveyance System, IEEE In Industry Applications Society Annual Meeting, 2008, 1-6.

[22] Kuo C. L., Li T. S. and Guo N. R., (2005). "Design of a Novel Fuzzy Sliding-Mode Control for Magnetic Ball Levitation System", Journal of Intelligent and Robotic Systems, 2005(42): 295-316.
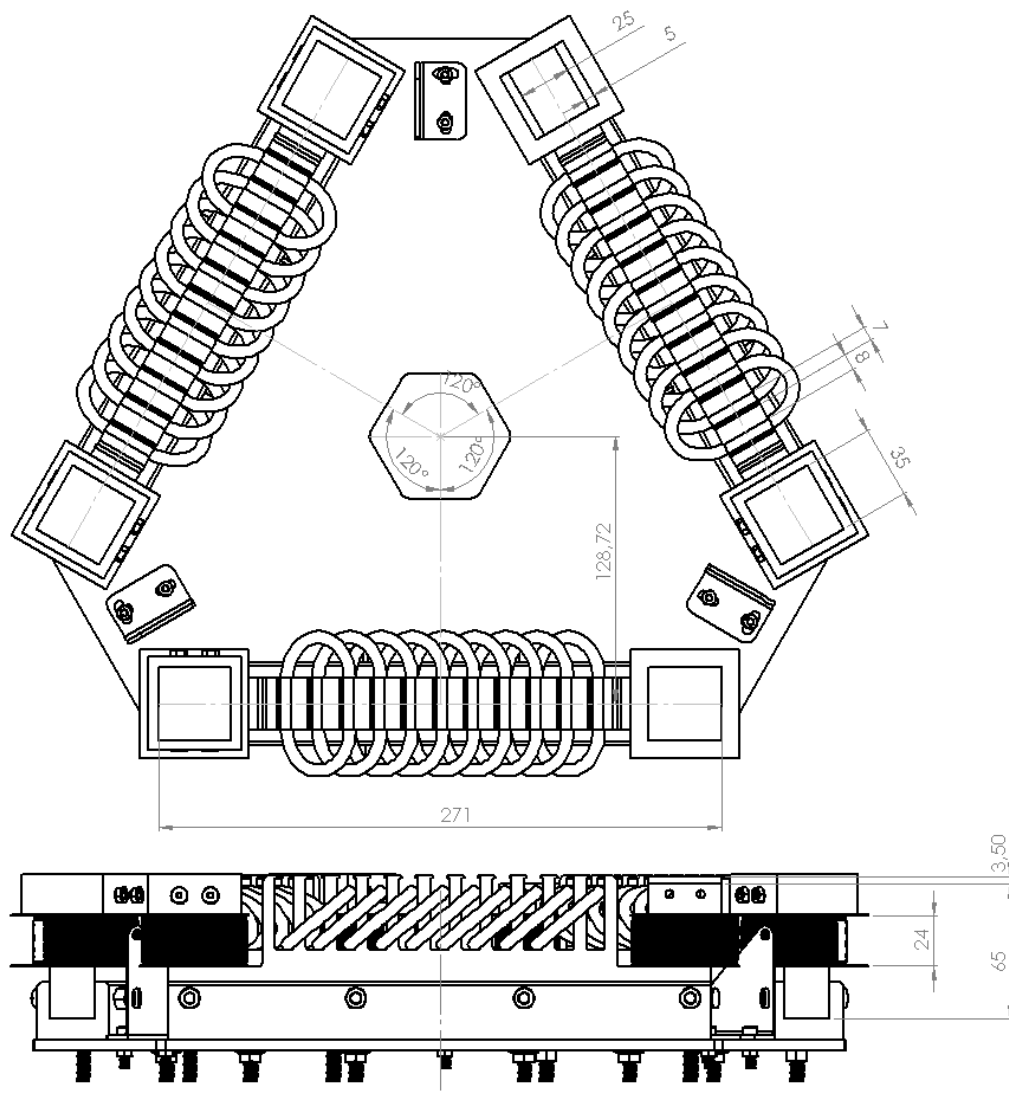
TECHNICAL DRAWING OF SYSTEM

Figure A.1 Geometric sizes of proposed system

CURRICULUM VITAE

PERSONAL INFORMATION

Name Surname	: Ahmet Fevzi BOZKURT
Date of birth and place	: 17/05/1990 Ankara
Foreign Languages	: English
E-mail	: afbozkurt90@gmail.com

EDUCATION

Degree	Department	University	Date of Graduation
Master			
Undergraduate	Mechanical Eng.	Yıldız Techical University	2013
High School		Haydarpaşa High School	2008

WORK EXPERIENCE

Year	Corporation/Institute	Enrollment
2011	TEPSAN Makina San. ve Tic. A.Ş.	Intern
2001	TEKNOVA Mekatronik Sistemler San. ve Tic. A.Ş.	Intern

PUBLISHMENTS

Conference Papers

1. ACEMP - OPTIM - ELECTROMOTION JOINT CONFERENCE 2015: Zero Power Control of a 6 DOF Levitated Multiple Hybrid Electromagnet Flexible Conveyor System (Ahmet Fevzi Bozkurt, Ömer Faruk Güney, Kadir Erkan)

2. ISEF 2015: 3-DOF Centralized I-PD Control of Nonlinear Magnetic Levitation System (Ömer Faruk Güney, Ahmet Fevzi Bozkurt, Kadir Erkan)

Projects

1. YÜLAP (2015-06-04-YL02): Doğrusal Endüksiyon Motorları ile Tahrik Edilen Manyetik Yastığın Sıfır Güç Yöntemi ile Kontrolü

2. KAP (2013-06-04-KAP01): Doğrusal Endüksiyon Motorları ile Tahrik Edilen Manyetik Yastıklama Temelli Esnek Taşıma Sistemi Tasarımı

3. TÜBİTAK (112M210): Planar Doğrusal Motorla Tahrik Edilen Manyetik Yastıklama Temelli Bir Esnek Taşıma Sisteminin Optimal Tasarımı ve Pozisyon Algılama Ağı ile Geri Beslemeli Pozisyon Kontrolü